Optical Techniques to Assess Cutaneous Microvascular Function in Cardiovascular Disease

Inka Mustajoki, Julien Riancho, Tuukka Panula, Jukka-Pekka Sirkiä, Jorge Herranz Olazabal, Smriti Badhwar, Maria Kjellman, Katri Karhinoja, Maria Maia, Sam Riahi, Yannis Papadopoulos, Evelien Hermeling, Rosa-Maria Bruno, and Matti Kaisti

(Methodological Review)

***Abstract*—Microcirculation is essential for maintaining tissue health and overall physiological function. Over the past few decades, various optical techniques have been developed to measure, visualize, and assess microvasculature. The skin has easily an accessible vascular bed allowing for noninvasive evaluation of microvascular function. Alterations in cutaneous microcirculation have been linked to dysfunctions in other target organs and vascular regions reinforcing the idea that cutaneous microcirculation can provide insights into systemic vascular conditions. Currently, there is no unified review focusing specifically on microcirculation-related optical techniques nor comprehensive analyses connecting these technological innovations to clinical evidence. This review aims to bridge that gap by systematically examining the wide spectrum of optical technologies used in assessing cutaneous microvascular function. We review techniques based on noncoherent light including oximetry, photoplethysmography, and microscopic methods and coherent light-based techniques, including speckle contrast imaging, diffuse correlation spectroscopy, photoacousting imaging, laser Doppler flowmetry and self-mixing interferometry. We emphasize cardiovascular research and evaluate the clinical relevance and technical maturity of the techniques. Additionally, brief explanation of skin structure and skin microvasculature while explaining light skin interaction is discussed. Lastly, we discuss these findings on wider context by including discussions and advancements in multimodal monitoring and machine learning.**

***Index Terms*—Cardiovascular disease (CVD), hyperspectral imaging (HSI), laser Doppler flowmetry (LDF), laser speckle contrast imaging (LSCI), microvascular function, near-infrared spectroscopy (NIRS), photoacoustic imaging, photoplethysmography (PPG).**

I. Introduction

MICROCIRCULATION refers to the blood circulation of the smallest vessels consisting of arterioles, capillaries and post capillary venules. The microvasculature is a terminal network of the systemic network, and it is responsible for regulating blood flow and pressure through vascular tone, maintaining tissue perfusion, oxygen transport and supporting cellular metabolism [1], [2], [3].

Changes in skin microcirculation have been associated with alterations in various target organs and vascular beds, reinforcing the idea that skin microcirculation can serve as a representative model for overall microvascular function [1], [4]. Dysfunction in skin microcirculation has been documented in individuals with cardiovascular disease (CVD) and those at increased cardiovascular risk, where it correlates with multiple risk factors. This suggests its potential use as a surrogate marker for vascular damage [5]. More specifically, impaired microvascular function has been linked to various conditions and diseases, including hypertension, microcirculatory dysfunction, heart failure, diabetes, and obstructive sleep apnea [6]. Furthermore, mechanisms behind the changes in cutaneous microvasculature and disease have been studied [7], [8], [9], [10]. For example, coronary artery disease patients have shown impaired microvascular function in reactivity tests performed with laser Doppler flowmetry (LDF) and laser speckle contrast imaging (LSCI) [10], [11] whereas hypertensive patients have shown reduced skin blood flow [12] and vasoreactivity [13], and impaired recruitment of perfused capillaries [14]. Moreover, finger microcirculation in congestive heart failure has been shown to deteriorate as a function of the severity and duration of heart failure [15].

Manuscript received 26 June 2025; revised 23 October 2025 and 24 November 2025; accepted 26 November 2025. This work was supported by the European Union's Horizon Europe Research and Innovation Programme under Grant Agreement 101115492. *(Corresponding author: Matti Kaisti.)*

Inka Mustajoki, Tuukka Panula, Jukka-Pekka Sirkiä, Maria Kjellman, Katri Karhinoja, and Matti Kaisti are with the Department of Computing, University of Turku, 20500 Turku, Finland (e-mail: mkaist@utu.fi).

Julien Riancho, Smriti Badhwar, and Rosa-Maria Bruno are with the INSERM, INSERM UMRS 970, Paris Cardiovascular Research Centre – PARCC, 75015 Paris, France.

Jorge Herranz Olazabal and Evelien Hermeling are with IMEC NL, 5656 AE Eindhoven, The Netherlands.

Maria Maia is with the Karlsruhe Institute of Technology (KIT), Institute for Technology Assessment and Systems Analysis (ITAS), 76133 Karlsruhe, Germany.

Sam Riahi is with the Department of Clinical Medicine, Aalborg UH, 9000 Aalborg, Denmark.

Yannis Papadopoulos is with the School of Applied Mathematical and Physical Sciences, National Technical University of Athens, 15772 Zografou, Greece.

Digital Object Identifier 10.1109/RBME.2025.3644411

TABLE I
SUMMARY OF REVIEWED TECHNIQUES FOR ASSESSING CUTANEOUS MICROVASCULAR FUNCTION, THEIR CLINICAL ASSOCIATIONS AND TECHNICAL DIFFERENCES

Technique	Principle	Site	Penetration depth	Parameters	Applications	Limitations	Relation w/age	Relation w/ disease	References
NIRS	Detect changes in hemoglobin oxygenation by spectroscopy in near-infrared light wavelengths (700-1100 nm)	Finger, toe	Perfusion, oxygenation, tissue oxygen saturation (StO_2), total tissue hemoglobin (HbT), tissue hemoglobin index (THI)	Reactivity test – tissue oxygen saturation at baseline and after reactive hyperemia, slope during occlusion and recovery	Brain oxygenation, flap monitoring StO_2	Other chromophores, penetration depth, motion artifacts	Yes	Peripheral arterial disease, insulin resistance, chronic kidney disease, COVID-19	[17], [18], [19], [20], [21], [22], [23], [24], [25], [26], [27], [28], [29], [30], [31]
VLS	Spectroscopy using visible light (400-700 nm)	Finger	on average 2 mm	StO_2, total superficial hemoglobin	Vascular monitoring, flap monitoring	Motion artifacts, other chromophores	No	Diabetes, diabetic foot	[32], [33], [34], [35], [36]
PPG	Measures changes in blood volume through absorption and scattering of light. Typically green (around 530 nm), red (around 670 nm), infrared (around 940 nm) wavelengths are used	Finger, ear, toe	Depends on wavelength (0.3 to 2.5 nm)	Various markers from the signal based on the wave shape, fiducial points, peak time, tissue optical perfusion pressure, augmentation index: SpO_2, perfusion, peripheral vascular tone, pulse propagation, heart rate, heart rate variability	Fitness trackers, clinical monitoring, anesthesia monitoring, critical care	Motion artifacts, specificity, subject variability based on skin tone	Yes	Hypertension, diabetes, peripheral arterial disease, COVID-19	[37], [38], [39], [40], [41], [42], [43], [44], [45], [46], [47], [48], [49]
HSI	Combines spectroscopic and imaging principles to produce 3D-data non-invasively without contact between monitor and tissue (400-1100 nm)	Lower limbs, foot, forearm, aorta	up to 20 mm	t Tissue hemoglobin index, near-infrared perfusion index, tissue water index, oxygen and hemoglobin saturation, oxyhemoglobin and deoxyhemoglobin levels	Disease detection, image-guided surgeries	Local tissue heterogeneity, external pressure	Yes	Diabetic foot, peripheral arterial disease	[50], [51], [52], [53], [54], [55], [56], [57], [58], [59], [60], [61]
Microscopy	Microcirculation visualized by tissue illumination and capturing light scattered by hemoglobin of red blood cells (530 nm (SDF), 548 nm (OPS))	Skin, nailfold, sublingual	0.3 mm	Capillary diameter, red blood cell (RBC) velocity	Functional capillary density, microcirculation monitoring during surgery	Contact pressure, movement artifacts, resolution, blood velocity, skin thickness	No	Peripheral vascular disease, diabetes	[62], [63], [64], [65], [66], [67]
LSCI	Using coherent light as the source, motions in tissue can be measured and visualized by analyzing reflected interference patterns (600-900 nm)	Forearm, finger	Up to 0.7 mm	Microvascular skin reactivity measured by baseline flux, peak flux and increase of flux from baseline to peak response after transdermal acetylcholine iontophoresis or other pharmacological or physiological provocations	Skin perfusion imaging	Multiple scattering, motion artifact	No	Hypertension, diabetes, chronic renal disease, dyslipidemia, coronary artery disease	[68], [69], [70], [71], [72], [73], [74], [75], [76], [77], [78], [79], [80], [81], [82]
DCS	Long-coherence light laser for emitting light is used to measure blood flow by analyzing the fluctuations in the intensity of reflected light (700 - 1100 nm)	Finger	Up to 15 mm	Perfusion/ blood flow monitoring, Reactivity test- Blood flow index, in combination with NIRS	Vascular monitoring, neuromonitoring, breast cancer	Signal-to-noise ratio	No	No	[83], [84], [85], [86], [87]
Photoacoustic imaging	Detects sound waves generated by excited targets by pulsed lasers and forms images of optical absorption.	Skin (finger, forearm, breast, neck etc), nailbed, brain	From superficial up to several centimeters depending on configuration	Provides structural, functional, and molecular insights such as hemoglobin, lipids, melanin.	Vascular imaging, breast imaging, dermatological imaging, vascular imaging	Fairly costly, complex and bulky equipment, long scan times	Yes	Peripheral arterial disease, peripheral ischemia, diabetes, cancer, psoriasis	[88], [89], [90], [91], [92], [93], [94], [95]
Laser Doppler flowmetry	Illuminating tissue with a monochromatic laser light and detecting the Doppler frequency shift caused by moving RBC	Finger, limbs, oral mucosa	Up to 1 mm	RBC flux and velocity	Tissue perfusion monitoring, microvascular flap vascularization	Output is in arbitrary units. High laser power required for deeper tissue penetration	Yes	Peripheral arterial disease, endothelial dysfunction, hypertension, chronic kidney disease	[8], [96], [97]
Self-mixing interferometry	Light reflected from tissue re-enters laser cavity producing interference signal. (785 nm, 1310 nm)	skin (finger etc.)	Up to few millimeters	Blood flow	Subcutaneous blood flow imaging, blood clot detection, skin change detection, eye monitoring	Motion artifact, skin color	No	No	[98], [99], [100], [101]

Consequently, the importance of assessing microcirculation has gained recognition in studies investigating the pathophysiology of CVD and the stratification of cardiovascular risk [16]. The skin, as an easily accessible vascular bed, offers a convenient site for non-invasive evaluation of microvascular function.

In this article, we review techniques for assessing cutaneous microvascular function, with a focus on those relevant to monitoring cardiometabolic diseases. We begin by outlining the principles of optical sensing, including the interaction between light and skin. This is followed by an overview of key optical techniques, encompassing both commercially available methods and those in the research phase. For each technique, we describe the operating principle and summarize recent medical evidence supporting its use. An overview of the techniques and their clinical relevance is presented in Table I. Finally, we briefly explore emerging research directions, such as multimodal monitoring and the integration of machine learning, before concluding with a discussion. Although several existing reviews discuss microvascular evaluation in general, they often encompass a wide range of techniques, including biochemical assays, various imaging approaches, and other non-optical modalities. In contrast, our review focuses exclusively on optical technologies, providing a unified work that integrates technical principles and recent clinical information within the optical domain. Furthermore, unlike previous reviews that address either technological aspects or clinical applications separately, our work tries to bridge these two dimensions.

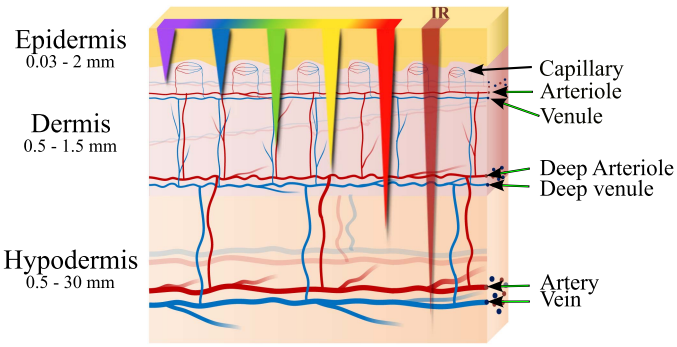

Fig. 1. The functional layers of the skin along with the structure of the blood vessels. The approximate penetration depth of light into skin is presented as an overlay.

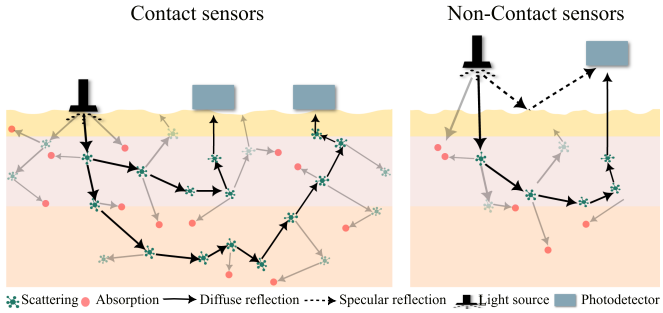

Fig. 2. Skin light interaction. As light travels through the skin, it may be absorbed by molecules, such as hemoglobin or melanin, or scatter across multiple points within the tissue. The scattered light that returns to the surface can then be detected by photodetectors or camera. Black lines indicate photon paths that reach the sensor and gray lines indicates those that do not reach the sensor.

II. Principles of Optical Sensing

A. Skin Structure and Microvasculature

The skin consists of three functional layers: epidermis, dermis, and hypodermis (see Fig. 1) [100]. The epidermis functions as the protective surface layer, forming a physical and chemical barrier against environmental factors. This bloodless layer varies greatly in thickness depending on body location, from less than 0.1 mm on the face to 1–5 mm on the soles of the feet [100]. Beneath the epidermis is the dermis that contains two important plexuses of cutaneous microcirculation: an upper horizontal network in the papillary dermis from which the capillary loops arise and a lower horizontal plexus at the junction of the dermis and the hypodermis below it. The two plexuses are connected by ascending arterioles and descending venules. The papillary dermis contains most of the microvasculature [2]. The deepest layer, the hypodermis, consists of connective tissue with fat cells, which together act as a cushion and a storage of energy [100]. The larger perforating blood vessels in the hypodermis connect to the lower plexus in the dermis [2].

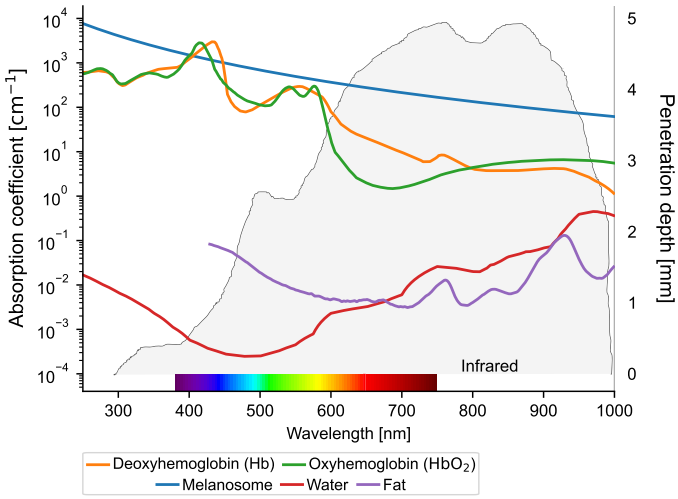

Fig. 3. Absorption spectra of skin chromophores. For microcirculation assessment, both oxygenated and deoxygenated hemoglobin are area of special interest but other chromophores have to be taken account. The approximate penetration of light to skin based on a simulation [106] is presented with gray hue. The hemoglobin spectra are adopted from https://omlc.org/spectra/hemoglobin/summary.html.

B. Interaction of Light With Skin

The interaction of light with the skin is determined by its optical properties. In a typical setup, a light source and a photodetector or camera are used to detect photons after their interaction with tissue. A clear distinction exists between contact and non-contact sensing methods. A non-contact setup is influenced not only by diffuse reflection, as in contact sensing, but also by specular (mirror-like) reflection from the skin surface, as illustrated in Fig. 2 [101]. Specular reflection does not carry any direct subcutaneous information and is usually removed during signal processing. These reflections are also sensitive to minor alterations in the optical path caused by body motion. Some of this motion originates from ballistic forces that repeat with each cardiac cycle. While these forces are used to record ballistocardiograms, they are generally considered noise in optical sensing. Notably, specular reflection can be the dominant component in the detected signal. In contrast, the diffuse reflection which is the primary component in contact sensing, is associated with the propagation of light within the skin.

Skin is a turbid medium, where light propagation is determined by reflection, refraction, scattering, and absorption. In the spectrum of visible light, approximately 4–7% is reflected by the surface of the skin, whereas the remaining portion is refracted [102], [103]. The refractive indices at the boundary of different media determine how light propagates from one layer to another [100]. During propagation, light undergoes scattering events caused by interactions with small regions that have optical properties different from the surrounding tissue, altering its direction [103]. Only a very small fraction of light is inelastically scattered (leading to a change in wavelength), whereas the vast majority is elastically scattered. The propagation can result in either photons escaping the skin into the outside medium (e.g., air) or absorption, where the photon energy is thermally dissipated [100].

In most soft tissues, penetration depth is primarily determined by their optical properties [104]. Fig. 3 illustrates the absorption spectra of endogenous tissue chromophores, highlighting the

strong wavelength-dependent attenuation of light in tissue. In the epidermis and dermis, absorption in the spectral range of visible light is mainly determined by melanosomes containing melanin and components of blood (hemoglobin and its derivatives) [100], [105] whereas water dominates in the near-infrared (NIR) range [100]. Scattering is higher in the epidermis than in the dermis or hypodermis due to the epidermal melanin content. In the dermis, scattering is dominated by collagen fibers, with collagen also playing a role in the scattering properties of the hypodermis along with elastin [100].

In general, the penetration depth of light into the skin increases with increasing wavelength in the visible-light range [106]. This is due to the decreasing absorption by melanin and hemoglobin [100]. At approximately 600 nm there is a steep decrease in the absorption of hemoglobin, resulting in a steep increase in penetration depth [106]. The penetration ability begins to decrease after approximately 900 nm [106], at which point the absorption of light due to water and lipids begins to gradually increase [100].

Penetration depth also strongly depends on source-detector separation where shorter distances probe superficial layers, whereas larger separations reach deeper tissues, such as the dermis or hypodermis, depending on wavelength. Signal attenuation has been found to be significantly affected by the scattering properties of blood and the probed tissue volume as well as photon path length reducing the amplitude [49], [107].

It has also been observed that probe contact pressure can significantly impact the depth of light penetration [108], [109]. Contact pressure influences significantly measurement characteristics in contact-based methods, especially affecting PPG signal quality [110]. While current devices lack effective solutions for these pressure-induced variations, non-contact techniques such as hyperspectral imaging eliminate this limitation. One explanation for deeper light penetration with increased pressure is that blood is pushed out of smaller vessels in the superficial layers at relatively low contact forces, reducing light attenuation by blood. Another, although smaller, effect is tissue compression altering the optical path of light by modifying the physical properties of tissue, such as reducing thickness and changing scattering characteristics. This combination of effects leads to variations in light penetration depth at different levels of contact pressure.

Light–tissue interaction is complex, and one common approach to estimating it is through Monte Carlo simulations [111], [112]. By incorporating the optical properties of skin into a tissue model, and the characteristics and geometry of both the light source and detector, it is possible to estimate the propagation path of light including penetration depth and to identify how different components in the system affect the propagation. A limitation of such simulations is their static nature, which does not account for the dynamic behavior of blood flow. The limitation of Monte Carlo simulation is in its static nature, which cannot account for the dynamic behavior of blood flow. However, recent advances in fluid-structure interaction algorithms, which couple blood flow dynamics to vessel wall mechanics and capture phenomena such as arterial compliance, wall deformation, and pressure wave propagation, may offer a means to overcome this limitation [113].

III. Techniques Based on Non-Coherent Light

A. Oximetry

Optical properties of hemoglobin vary depending on its oxygenation state resulting in distinct absorption spectra for oxygenated and deoxygenated hemoglobin (see Fig. 3). Pulse oximetry is a technique based on photoplethysmography (PPG) which estimates peripheral oxygen saturation (SpO_2), that describes percentage of oxygenated hemoglobin in circulatory blood. Pulse oximeters measure the pulsatility of the blood and use different parts of the signal to determine changes in light absorbance [114], [115]. Whereas SpO_2 is used as an estimate of percentage of oxygenated hemoglobin in systematic circulation, StO_2 (tissue oxygen saturation) evaluates locally oxygenation level of arterioles and other superficial vessels of tissue. Thus, StO_2 does not need the pulsatile component of the PPG. Besides of red and infrared wavelengths used in pulse oximeters, StO_2 can also be obtained with shorter wavelengths, because focus is on the most superficial vessels (see Fig. 3). StO_2 values in normal, healthy, state varies from as low as below 60% to over 90%. The range of StO_2 values depends highly on the measurement site and tissue as well as used device [116], [117], [118].

An important clinically relevant application of StO_2 is tissue flap monitoring. Traditionally the reconstructed flaps are monitored by medical personnel with a hand-held Doppler ultrasound device and other (visual) evaluation criteria, which do not allow continuous monitoring of the flap leading to greater probability of failure. StO_2 devices enable continuous monitoring of skin flaps and decreases risk of failure [58]. Clinically StO_2 is measured using either near-infrared spectroscopy (NIRS) [119] or visual light spectroscopy (VLS) (for example T-Stat, Spectros Medical Devices, USA) [120].

1) Near-Infrared Spectroscopy: Light spectroscopy studies the composition of matter by examining how it interacts with electromagnetic radiation. This interaction generates a spectrum, a pattern of light intensities across different wavelengths, that is indicative of the optical properties of the material being studied. By analyzing this spectrum, molecular, chemical and physical properties of tissue can be studied and quantified [121], [122]. Light spectroscopy techniques that uses wavelength in the range of 700 to 1100 nm are called near-infrared spectroscopy (NIRS).

NIRS has been used for free flap oxygenation monitoring and detection of decreased tissue perfusion, and it has been reviewed in several papers [25], [123], [124]. NIRS provides a higher skin flap salvage and overall flap survival rate compared to clinician's assessment only because compromised blood flow in the skin can be more easily detected. NIRS has also been used with a vascular occlusion test (VOT) to evaluate microvascular function in different populations. VOT involves supra-systolic occlusion at the measurement site for 5 minutes and comparison of the changes in StO_2 kinetics before and after the release of occlusion.

NIRS-derived indices of microcirculatory function measured at the forearm have been reported to be reduced in middle aged and elderly compared to young participants [17], [18], [19]. A difference between sexes has also been reported in

NIRS-derived StO_2. Females show greater reperfusion rates at both forearm and quadriceps as compared to males [125]. In a study comparing NIRS-derived indices measured at the foot, patients with peripheral arterial disease (PAD) showed significantly impaired microvascular function compared to age-matched healthy controls [20]. Microvascular responsiveness may be altered in CVDs and conditions with increased risk of CVD [21], [22]. The effects of COVID-19 and post-COVID-19 symptoms even after recovery (long-COVID) on the vasculature has been well established. Evidence of microvascular dysfunction was reported in patients of COVID-19 during a VOT using NIRS [23]. Furthermore, using the same technique, patients with long-COVID showed an impaired microvascular responsiveness during the occlusion phase of VOT compared to patients with CVD [24].

Despite the wide use in clinical setting, NIRS has some drawbacks. Currently, the use of NIRS is limited to cutaneous measurements from the skin, since the sterility of the measuring probe cannot be guaranteed [58]. In addition, NIRS shares the typical challenges of spectroscopic measuring techniques, such as the effect of melanin and error caused by external light irradiation. Furthermore, NIRS is not limited to microcirculation, as NIR light penetrates up to 5 mm to skin, measuring information from both micro- and macrovasculature.

2) Visible Light Spectroscopy: Visible light spectroscopy (VLS) relies on visible light (wavelengths between 400 nm and 700 nm) in vascular monitoring. Since VLS uses visible light, it is shallow-penetrating and thus monitors local blood flow in smaller vascular structures. Only penetrating 2 mm into the tissue on average, VLS is used to measure capillary saturation, whereas near-infrared wavelengths measure the overall oxygenation in arterial, venous and capillary vascular compartments [33].

Combination of VLS and NIRS is used in commercial Spatial frequency domain imaging (SFDI) system, and with that different microcirculatory patterns were observed in two patients with neuropathic vs neuro-ischemic diabetic foot ulcers [32].

VLS requires a significantly smaller volume of tissue to monitor the blood flow compared to NIRS [34], [35]. Another advantage of VLS compared with NIRS is the narrower normal range in oxygenation percentages ($\pm$ 3% and $\pm$ 9%, respectively) [36]. Thus, the advantages of VLS is its potential to monitor oxygenation in significantly smaller tissue volumes and to be incorporated to small structures such as pins or needles to monitor the oxygenation *in vivo*. This advantage results from smaller penetration depth, however, this also limits the use of VLS to only the very surface of the tissue of interest.

B. Photoplethysmography

Photoplethysmography (PPG) is a non-invasive optical monitoring technique widely used in both clinical and health/activity monitoring settings, providing information ranging from physiological parameters to the assessment of vascular and autonomic functions [44]. A PPG signal can be acquired from the skin using inexpensive and widely used components, a light-emitting diode (LED) and a photodetector [45]. Traditionally PPG is recorded using a sensor in direct contact (contact PPG) with the skin. However, using an RGB camera PPG waveform can be collected from a distance (remote PPG).

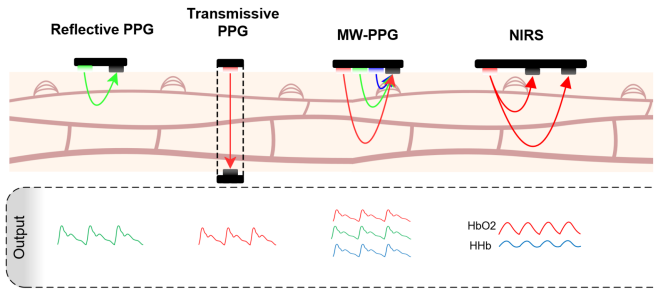

Fig. 4. i) Reflectance mode PPG sensor. ii) transmission mode PPG, iii) MW-PPG configuration with three wavelengths. iv) NIRS configuration with an NIR light source and two photodetectors at different distances.

The operating principle of PPG relies on absorption of light by hemoglobin contained in the blood. The increased blood volume absorbs more of the light illuminated by the light source, leading to a decrease in the light intensity registered by the photodiode and thus a decrease in the PPG signal. Consequently, the subsequent decrease in peripheral blood volume during diastole leads to an increase in the PPG signal. The resulting cyclic and pulsatile part of the PPG signal, reflecting the activity of the heart, is commonly referred to as the AC (alternating current) component. This component is superimposed onto a significantly larger but slowly varying baseline, commonly referred to as the DC (direct current) component. The DC component is related to non-pulsatile absorption of light, such as average blood volume and tissues, and its level varies due to respiration, sympathetic nervous system activity, and thermoregulation [46].

PPG is widely adapted and studied technique, foremost due to the simplicity of the technique. A PPG signal can be acquired from the skin using inexpensive and widely used components [45]. The reliability of PPG measurements is challenged by various factors affecting signal quality. These include absorption variations due to skin chromophores (e.g skin color), perfusion changes caused by temperature fluctuations, motion artifacts, and measurement instability from varying contact pressure [126]. Different combinations of visible-to-infrared wavelengths have been proposed to address the challenges [127], [128], [129].

1) Contact Photoplethysmography: The light source and the photodiode can be placed either on the same side of the skin (reflection mode), or on the opposite sides of a sufficiently thin body part (e.g., a fingertip or an earlobe), known as the transmission mode [44], [46]. Fig. 4 illustrates operating modes of PPG. In a transmission-mode PPG sensor, the photodiode detects light that passes through the body part, whereas in reflection-mode, the photodiode captures light that is backscattered and reflected from the tissue. Reflection-mode PPG sensors are widely used in

commercial products due to their versatility, allowing placement on various body sites such as the wrist and finger.

While traditional PPG uses a single wavelength to probe arterial blood, multiwavelength PPG (MW-PPG) combines multiple light sources to target different layers of skin vasculature [130]. A common approach is to combine three wavelengths in the approximity of red, infra-red and green lights, which are often used in wearable devices. Sensor manufacturers offer a variety of integrated PPG sensor packages with this combination of LEDs. Recently, a system combining an MW-PPG sensor with a mechanism to control sensor contact pressure has been proposed to estimate mean blood pressure at different depths of the skin. Such a system allows estimation of blood pressure not only from large arteries located deep in the skin, but also from smaller, more superficial vessels of the microcirculation [108], [109].

The shape of the PPG waveform can provide information about the status of the microcirculation in health and disease. Changes in the shape of the PPG waveform have been described with respect to age and location of the sensor on the body [37]. There is a rightward shift in the peak of the pulse wave and diminishing of the dicrotic notch with increasing age [37]. Similar alterations are observed in PPG of patients with vascular damage such as hypertension, diabetes and peripheral arterial disease [38], [39], [40]. Nitroglycerin administration is able to normalize wave shape in hypertensive patients [38]. In children and adolescents with Type 1 diabetes, microcirculatory PPG were observed in those with neuropathy [39], whereas in middle-aged and elderly patients with Type 2 diabetes PPG curve shape alterations are visible regardless of microangiopathy [41].

PPG has also been used to evaluate microvascular dysfunction in cardiac and systemic vascular diseases. The change in PPG in response to exercise was lower in patients with myocardial ischemia as opposed to those without ischemia indicating impaired peripheral microcirculation in these patients [131]. Peripheral microcirculation can also be impaired due to alteration of cardiac rhythm such as with atrial fibrillation. PPG based measurement of microcirculation has been used to evaluate the improvement in microcirculation after restoration of sinus rhythm by cardioversion [132]. In conclusion, changes in microvascular function with aging and cardiovascular risk factors are associated with alterations in PPG wave shape although there is no clear evidence on the specificity and clinical utility on these changes.

2) Remote Photoplethysmography: Remote PPG (rPPG) applies the principles of PPG to a remote monitoring system using a camera instead of a direct-contact sensor (see Fig. 5) [47], [133]. In essence, it enables contactless monitoring in situations where maintaining physical contact with the PPG sensor is impractical or difficult, such as when driving a car [134] or monitoring a neonate in an incubator [135].

The cameras used for rPPG range from high-speed imaging systems to low-cost webcams, typically operating at sampling rates of 30 frames per second or less [136]. Most studies use cameras with standard red, green, and blue (RGB) channels, although specialized setups such as five-band cameras [137] and NIR cameras [138] have also been explored. Illumination can range from ambient light to artificial sources or a combination of both [136].

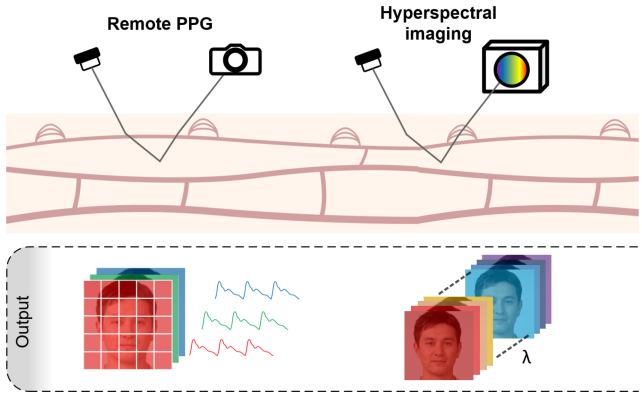

Fig. 5. Remote non-coherent techniques. Remote PPG uses a CMOS/CCD camera to capture the pulsatile waveform from different areas of the image. Red, green and blue channels are often recorded. Hyperspectral imaging extends the channel count to allow recording in hundreds of wavelengths.

The process of converting video frames into a plethysmogram involves signal extraction and estimation [48]. In signal extraction, a region of interest (ROI) is detected and tracked using machine learning techniques. The color channels of each frame within the ROI are then spatially averaged to calculate the raw signals [47], [48]. In the signal estimation phase, the signals are filtered, and a channel or combination of channels is selected for further processing using methods such as principal component analysis (PCA), independent component analysis (ICA), or model-based approaches [48], [136]. Heart rate is the most commonly derived parameter, but rPPG signals have also been used to calculate heart rate variability, respiratory rate, and SpO_2, as well as to detect atrial fibrillation [139].

C. Hyperspectral Imaging

Hyperspectral imaging (HSI) combines spectroscopic and digital imaging principles to produce three-dimensional data. As traditional cameras capture the red, green, and blue frequency bands, a hyperspectral camera is able to capture more channels across the electromagnetic spectrum - wavelengths ranging from visible to near-infrared light. The terms hyperspectral and multispectral imaging are often used interchangeably, but they differ in the number of spectral bands they capture. The principles of HSI have been described in detail in [51]. The principle of hyperspectral imaging is shown in Fig. 5.

HSI provides various outputs depending on clinical requirements, including StO_2, tissue hemoglobin index, near-infrared perfusion index, and tissue water index. Tissue hemoglobin index quantifies the relative amount of hemoglobin within the tissue volume of interest. Additionally, the near-infrared perfusion index reflects oxygenated hemoglobin in the microcirculation of underlying tissue, while the tissue water index indicates the relative water content within the total tissue volume. In summary, HSI offers an objective, precise, and reproducible approach to assessing tissue perfusion and hemoglobin oxygenation [50], [58], [60], [61].

In medicine, HSI is used to non-invasively and without skin contact to monitor tissue oxygenation saturation [59]. HSI has

been studied on PAD in the lower limbs. Studies have demonstrated the effectiveness of HSI in differentiating ischemic areas from regions with normal blood flow [51]. PAD has also been evaluated against common clinical practice and a significant correlation was shown with transcutaneous oxygen measurement (TCOM), ankle brachial index (ABI), and skin temperature [52]. HSI parameters have been correlated with disease severity represented by the Rutherford classification as well as in diabetic patients with neuropathy [53]. In addition, it has been shown that HSI could predict healing of diabetic foot ulcers [54], [55], [56] HSI could therefore be a valuable tool for assessing ischemic lesions and monitoring the progress of tissue healing. Although HSI has not yet been implemented into routine clinical use, these results demonstrate the potential of HSI in various clinical scenarios. Furthermore, to date, no study has correlated HSI with the presence of different cardiovascular risk factors (hypertension, dyslipidemia, diabetes, arterial stiffness) to predict the occurrence of cardiovascular events. HSI has been studied against NIRS in free flap monitoring, compared with clinicians assessment, which is still the gold standard. In a review study [58] there was no clear difference between NIRS and HSI performance, and neither outperformed clinical flap evaluation.

One advantage of HSI is its ability to measure without direct skin contact. This provides the opportunity to use HSI in for example operating rooms, where sterility is mandatory and thus techniques requiring skin contact cannot be used. Contactless measurement also allows for a larger surface area to be measured. HSI outperforms methods that only measure blood flow because of its ability to differentiate oxygenated and deoxygenated hemoglobin. Since tissue perfusion can be unaffected while oxygenation is compromised, HSI answers the critical question of oxygen supply to the tissue of interest rather than only measuring the blood flow [140]. The high cost of HSI systems—starting at approximately USD 10,000 per camera—limits their widespread adoption. Moreover, the large volume of collected data slow down processing, restricting real-time analysis capabilities [59].

D. Microscopy

Microscopy is a technique that uses optical systems to magnify and visualize structures too small to be seen with the naked eye. Light microscopy has multiple applications in the context of microvascular monitoring. Nailfold capillaroscopy, orthogonal polarization spectral imaging and dark field imaging techniques share characteristics such as using visible light excitation and optical magnification to capture images. Furthermore, all these techniques enable both structural and dynamic assessment of microcirculation.

Microscopic techniques have limitations. While they do not require laser optics, the inclusion of high-magnification components introduces additional cost and optical complexity to the system. Furthermore, because the system operates within the visible light spectrum, its penetration depth is restricted compared to NIR–based techniques. In the case of nailfold capillaroscopy, the technology is applicable only to the nailfold region of the microvasculature, limiting its use in assessing other tissue sites.

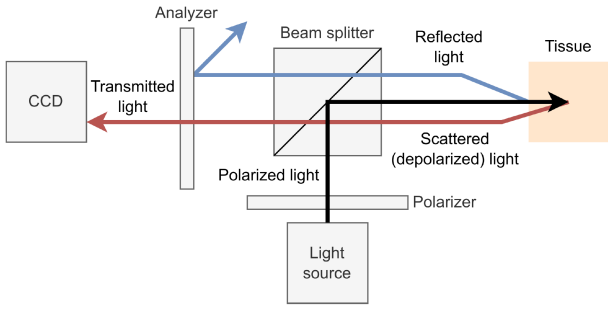

Fig. 6. Optical schematic of an OPS configuration [62]. Tissue is illuminated with linearly polarized light, and the camera detects only the orthogonally polarized component of the backscattered light.

1) Nailfold Capillaroscopy: Nailfold capillaroscopy uses visible light microscopy to assess the microvasculature at the base of the fingernail [67]. At the nailfold, capillary loops run parallel to the skin surface, unlike in other cutaneous tissues where they are oriented perpendicularly. This makes the nailfold an ideal site for direct visualization of capillary loops. The procedure can be done using a traditional stereomicroscope or by videocapillaroscopy, where the results can be accessed on a computer. The parameters assessed for clinical use include the density, diameter and morphology of the capillary loops as well as hemorrhaging. These parameters can be used to differentiate between sclerodermic and non-sclerodermic patterns. In addition to structural imaging nailfold capillaroscopy has been used to obtain blood flow dynamics by evaluation of moving red blood cells (RBC) via high-speed imaging [141] . The usage of nailfold capillaroscopy has been clinically established for the diagnosis of systemic sclerosis and Raynaud's phenomenon, but lately it has been proposed for assessing e.g. diabetes and CVDs, such as heart failure [142], [143], [144].

2) Orthogonal Polarization Spectral Imaging: Orthogonal polarization spectral (OPS) imaging employs linearly polarized light in combination with a polarizing beam splitter and a lens to illuminate a small circular area of skin, approximately 1 mm in diameter. Light reflected and backscattered from the tissue passes through the beam splitter and an orthogonal polarizer positioned behind it before reaching a video camera. The orthogonal polarizer blocks most of the directly reflected polarized light, while allowing depolarized light, which has undergone multiple scattering events within the tissue, to pass through. This process effectively back-illuminates absorbing structures, such as blood vessels containing light-absorbing red blood cells, enhancing their visualization [62], [63]. Optical schematic of an OPS configuration is illustrated in Fig. 6. The recorded videos can be analyzed to measure functional capillary density, RBC velocity, and small blood vessel diameter [62], [145]. OPS can be used in clinical setting for measurement of functional capillary density (FCD), and that has been validated against conventional capillary microscopy [63].

3) Dark Field Imaging: Sidestream dark field (SDF) imaging uses a ring of LEDs perpendicular to the skin and arranged concentrically around a light guide connected to a video camera. The light guide focuses the LED light beneath the

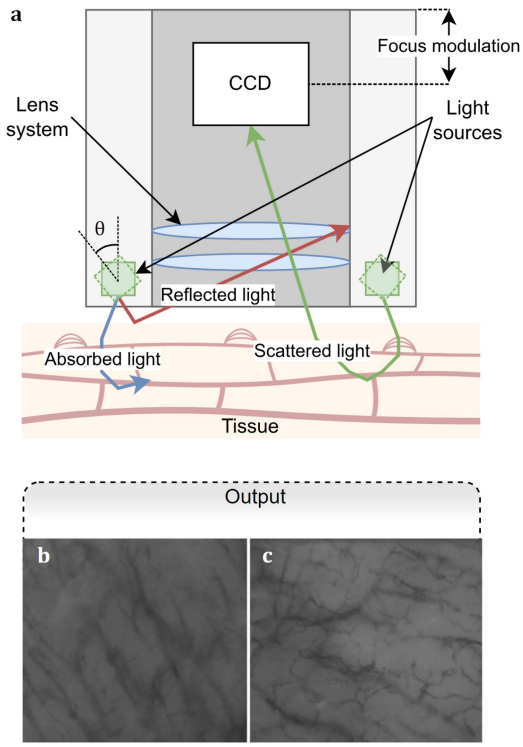

Fig. 7. Operating priciple of dark field illumination techniques. (a) Probe configuration. The angle (θ) of the light source is the differentiating factor in SDF and IDF [64]. (b) and (c) Outputs from SDF and IDF, respectively. Microphotographs adapted from [148].

blood vessels and blocks specular reflection from the tissue surface, ensuring optical insulation between the light guide and the illuminating LEDs. Photons entering the light guide result from scattering within the tissue, and similar to OPS, absorbing structures like RBCs appear dark against a white or grayish background. To enhance image quality, the LEDs are pulsed in synchronization with the frame rate of the camera, capturing the motion of RBCs more effectively. The LEDs emit light at a central wavelength of 530 nm, the isosbestic point of oxygenated and deoxygenated hemoglobin, ensuring light absorption is independent of the RBC oxygenation state while providing optimal contrast [64]. SDF is regarded as the second generation of hand-held microscopes relative to the OPS technique [146].

Compared to SDF, in incident dark-field illumination (IDF) the LEDs are positioned at an angle to utilize the principles of dark-field illumination described in [65]. The measurement system is otherwise very similar to that in SDF but the angled LEDs ensure that only scattered light reaches the light guide [147]. SDF and IDF measurement system is shown in Fig. 7. IDF is considered as the third generation of hand-held microscopes [146].

There are few commercial devices using either SDF or IDF in the market, mainly for sublingual microcirculation monitoring [146]. Those devices can not be used for clinical decision making but are useful tools assessing blood flow in the most superficial blood vessels.

IV. Techniques Based on Coherent Light

A. Laser Speckle Contrast Imaging

Laser Speckle Contrast Imaging (LSCI) refers to a noninvasive optical technique which makes use of the reflection of coherent light to measure movement in tissues. Coherent light, e.g. produced by a laser source, is formed by photons coherent in wavelength and phase. These photons have the possibility to interact between each other producing a pattern of constructive and destructive interference at the target tissue. This effect is known as speckle pattern [79]. These photonic interferences fluctuate at the velocity of the scattering particles of the target volume, where the speckle is formed. In other words, when the target volume is static the speckle pattern will not fluctuate. When this pattern is recorded by a sensor, e.g. complementary metal-oxide-semiconductor (CMOS), the fluctuations of the speckle are perceived as blurriness, which is related to velocity. This technique allows for the measurement of two-dimensional tissue perfusion maps [80]. Furthermore, addition of time-frequency analysis enables examination of physiological mechanisms of blood flow changes [149], [150].

Although the initial use of LSCI in the medical field was mainly for retinal and cerebral applications, in recent years, LSCI has begun to be used in the cardiovascular field, particularly through research to assess microvascular function. This includes the assessment of microvascular skin perfusion (MSP), especially in patients with cardiovascular risk factors and those with established CVD. Several studies support the association between MSP and cardiovascular risk. When one of the major cardiovascular risk factors is present (hypertension, dyslipidemia, diabetes, or chronic kidney disease), MSP measurement using LSCI appears to be reduced. More specifically, several studies have shown that basal flow measured by LSCI and peak flow stimulated by various stimuli, in particular transdermal acetylcholine iontophoresis, as well as by other pharmacological or physiological provocations, are reduced in the presence of one of these risk factors [71], [72], [73], [74]. LSCI has also been studied in patients with CVD although data remain limited. Data show that it is significantly reduced in patients with coronary artery disease compared with healthy individuals, and this reduction is reversible with appropriate cardiac rehabilitation [11], [75], [76]. Furthermore, in a recent study LSCI was proven to be potential for early diagnosis of PAD and diabetic foot neuropathy [151].

Advantages of LSCI include combined microvasculature visualization and potential to measure quantitive perfusion data [149], achieved with real-time monitoring of local blood flow variations through high frame rate imaging [151]. However, the higher frame rates and image resolutions required in some applications increase data volume, leading to greater system complexity, higher costs, and computational delays in real-time monitoring, which may limit the use of this technology [152]. Additionally, working with lasers poses more safety considerations compared to LED-based techniques.

1) Speckle Plethysmography: Measuring LSCI in close contact with tissue does not allow for useful two dimensional perfusion maps. However, these images can be converted to

time signals, which are referred to as Speckle Plethysmography (SPG) [153], [154], [155]. The variation of SPG signals is related to the movement of blood cells, blood vessels and other tissue cells. At different wavelengths the penetration of light varies depending on the absorption and scattering coefficients of the tissues. Consequently, SPG signals variations will originate in the tissue parts where the light can reach. At short penetrating wavelengths, the variation of the SPG signal will originate in the superficial layers of tissue, whereas with longer wavelengths, the SPG signal will also be affected by deeper tissue layers. The behavior of two different wavelengths (639 nm and 850 nm) has been examined, showing how PPG and SPG of different wavelengths contain different information [155], [156]. An advantage of SPG systems is that they can provide with simultaneous PPG signals, processed from the same photons. Both SPG and PPG can either be measured in reflection or transmission. Reflection stands for the measurement mode in which the light source photons reflect onto a tissue, giving light intensity back in a direction determined by Snell's law. In this case an objective speckle pattern is generated at surface level, formed by the photons that reflect and scatter. In transmission, the light has to diffusely transmit from the light source to the detector through the skin and no detected photons are directly reflected. It has been shown that the information in reflection and transmission is different in a specific wavelength [155]. Another distinction can be made about SPG and PPG, while SPG depends on the concentration and velocity of scattering particles in the medium, PPG depends on the concentration of chromophores, which influences the amount of absorbed photons. A direct effect of this property is that PPG is inherently affected by ambient light changes, while SPG remains unaffected [154]. These differences can affect SPG and PPG signals producing waveform differences between them, which can be exploited [156]. The waveform of SPG signals have shown high correlation with continuous blood pressure [156], [157].

B. Diffuse Correlation Spectroscopy

Diffuse correlation spectroscopy (DCS) has gained significant popularity in recent years [81], [158], [159]. In typical DCS implementation, a long-coherence laser in the NIR range is used to illuminate tissue using a single mode fiber. The reflected light intensity fluctuations are recorded with photon counting device such as avalanche photo diodes, photomultiplier tubes and also CMOS detectors. The intensity fluctuations are considered to originate from moving scatterers, such as red blood cells. The resulting signal is then routed to either a hardware or software correlator to quantify the motion. The correlation of rapidly moving scatterers results in a shorter delay in the autocorrelated signal compared to slower-moving scatterers. Similarly, increasing the source-detector separation distance reduces the delays compared to shorter separations [159]. The majority of studies fit the autocorrelated signal into an analytical model to extract a blood flow index [81]. Although, the origin of the DCS signal remain somewhat elusive, the blood flow index extracted from DCS has been shown to be reliably proportional to cerebral blood flow estimates [160], [161].

DCS has been used in vascular monitoring, especially in neuromonitoring measuring blood oxygenation through the skull but also in breast cancer [162], [163], muscular monitoring [164], [165], and animal models for different pathologies [166], [167], [168].

Evidence for DCS-based assessment of cutaneous microvascular function is limited to a study in DCS is coupled with NIRS in vascular occlusion tests. NIRS-DCS system can monitor tissue oxygen saturation and microvascular blood flow during physiological changes such as exercise [169]. The results show that microvascular perfusion can be separated from convective oxygen delivery. The benefit of this setup is that both DCS and NIRS can be recorded with the same instrument by optical multiplexing of the laser sources. This requires the autocorrelation function to be performed digitally in the software rather than hardware, which reduces the temporal resolution.

The benefits of DCS are in part similar to other light spectroscopic methods: a non-invasive method for deep-tissue perfusion monitoring, also straight-forward hardware implementation without a need for calibration or gain adjustments. Despite many advantages, DCS is not free of drawbacks. One significant limitation is signal-to-noise ratio and difficulty to define and interpret absolute blood flow values [81].

C. Photoacoustic Imaging

Photoacoustic imaging (PAI), also known as optoacoustic imaging, is a non-invasive biomedical imaging technique that combines the high spatial resolution of optical imaging with the deep tissue penetration of ultrasound. It generates ultrasonic waves by irradiating tissue with nanosecond pulsed laser light to heat molecules to cause thermoelastic expansion which generates acoustic waves. Absorption in tissue takes place by chromophores — such as hemoglobin, melanin, water, or lipids that rapidly convert energy into heat, causing a small temperature rise. This leads to a pressure increase that relaxes, emitting low-amplitude acoustic waves [92], [104], [170]. The resulting sound waves are detected by either a single mechanically scanned ultrasound receiver or an array of receivers and are used to reconstruct images, based on the time of arrival, that reflect the distribution of light energy absorption within the tissue. Sound scatters significantly less than light and acoustic signals travel farther in tissue with minimal attenuation [92], [104].

In addition to visualizing anatomical structures like the microvasculature, PAI can also provide functional information, including blood oxygenation, blood flow, and temperature. The technique offers high spatial resolution across a wide range of length scales, from micrometers to centimeters, making it suitable for imaging both small and large structures.

There are several variants of PAI depending on chosen illumination and detection methods have broad range of depths and resolutions. Photoacoustic tomography achieves sub-millimeter resolution at depths of several centimeters, whereas photoacoustic microscopy can have sub-micron resolution with penetration depths of a few hundred microns [93]. A specific implementation most suitable to image and quantifying capillary network is the optical resolution photoacoustic microscopy (OR-PAM)

due to its submicrometer resolutions [91]. Algorithm related data compression sensing with reduced number of signals and hardware complexity has also been reviewed [171]. Some of the recent technological innovations include second to millisecond scan times allowing volumetric imaging of microvascular structures and dynamic 3D visualization of tissue perfusion [172], volumetric imaging of hemodynamics in vasculature up to few millimeters below the skin surface [173] and massively parallel ultrasonic transducers for human brain imaging [174].

PAI has broad applications in clinical medicine, preclinical research, and basic biological studies, and has been extensively reviewed [92], [93] and more specifically e.g. for cardiovasvular diseases [87], cancer [88], abnormalities in microcirculation [91], microscopy hemodynamics [175], and diabetes [89], [90]. In a proof-of-concept study the subcutaneous finger tissue in systemic sclerosis patients had clearly lower HbO_2 and HbT values [176]. In a similar study it was demonstrated that arteriovenous and venous vascular malformations could be investigated through quantification of oxygenated and deoxygenated hemoglobin before and after treatment [177]. In another pilot study PAI was used to assess tissue oxygenation in the nailfold and a greater drop in oxygen saturation was observed after cold stimuli in Raynauds's patients compared to healthy controls [178].

PAI combines great spatial resolution and penetration depth with high optical contrast and minimal speckle artifacts. While capable of measuring multiple parameters including hemoglobin concentration, blood flow, and oxygen metabolism, clinical applications typically focus on one or two parameters [175].

D. Laser Doppler Flowmetry

Laser Doppler flowmetry (LDF) is a technique based on illuminating tissue with a monochromatic laser light and detecting the Doppler frequency shift caused by moving RBCs scattering the light [179]. Most of the light scatters back from stationary cells and only a small portion of the light is affected by the Doppler shift. However, due to the spectral purity of the laser light these small variations can be detected. The concentration of the RBCs affects the fraction of Doppler-shifted light, whereas the average velocity of the RBCs affects the magnitude of frequency broadening. However, commercial LDF systems report only a single value that, under ideal conditions, reflects the product of these two properties of RBCs [180], [181]. Differences in LDF, LSCI and PAI outputs and measuring principles are shown in Fig. 8. The recorded values, or flux, are reported in arbitrary units, i.e. the technique is not able to provide values in absolute, physiologically meaningful units [181]. Monte Carlo modeling has shown that the penetration depth of LDF is less than 1.0 mm [180]. Penetration depths higher than this have been experimented with. This can be achieved using a longer-wavelength near-infrared laser and a longer emitter-to-detector distance [182]. However, this poses a problem with the need for a higher powered laser, and extra care has to be taken to keep the energy at a safe level.

LDF can be extended to include spatial information rather than just a single measurement point using a scanning mirror.

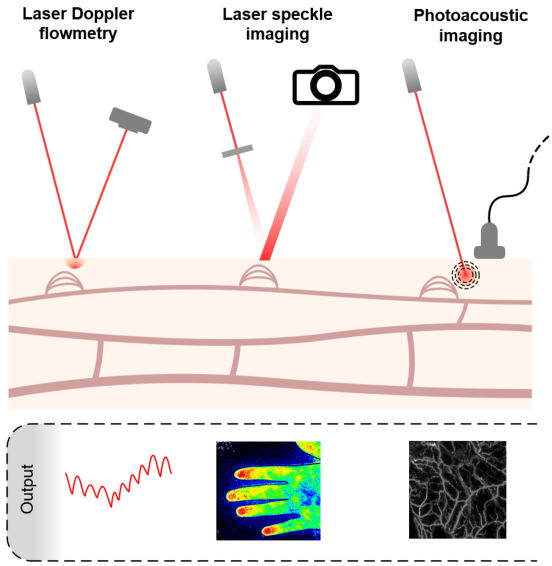

Fig. 8. i) LDF configuration using a laser light source and a photodetector, ii) Laser speckle imaging using a laser light source and a digital camera to observe the speckle pattern. Perfusion map adapted from [186] iii) Photoacoustic imaging using a laser light source and an ultrasonic transducer.

This is called Laser Doppler Perfusion Imaging (LDPI) [183]. The laser light is scanned over a rectangular area, giving spatial information about blood perfusion in the tissue.

Parameters derived from LDF signals have been associated with many CVDs, such as PAD, chronic kidney disease (CKD) and hypertension [8], [94], [95], [184]. More specifically, some research shows that microvascular skin reactivity is inversely related to the severity of cardiovascular risk as determined by the Framingham risk score in healthy female cohort but also in patients at high cardiovascular risk [7], [68]. Additional data show that skin microvascular reactivity is an independent predictor of atherosclerotic lesions and CVD in diabetic patients [69], [70]. In addition, it is inversely correlated with systolic blood pressure, highlighting the potential deleterious association between these two parameters [68]. Furthermore, in a clinical study LDF was demonstrated to be useful in monitoring peripheral vascular disease, especially chronic limb threatening ischemia [185].

LDF provides non-invasive, real-time assessment of microcirculatory perfusion and its rapid changes. Technique is limited by motion sensitivity by motion induced artifacts, relative perfusion values, and variations due to tissue optical properties [183]. Additionally LDF is limited to only single point measurement at the time.

E. Self-Mixing Interferometry

Interferometry is a method which uses the coherent property of laser light in order to measure distances, motion and/or structures of objects. The laser light is separated in two different optical paths with one being the reference path and the other being the optical path to which laser light is reflected by the target being measured. The light from the two optical paths is

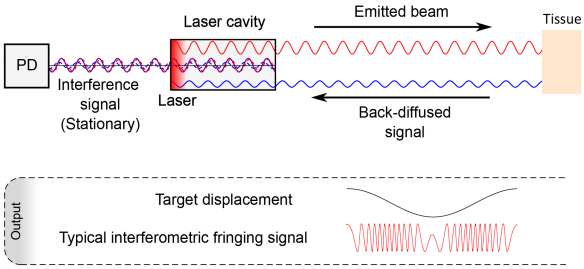

Fig. 9. Illustrative figure of SMI. A small fraction of the laser light emitted from the laser cavity is reflected back from a target and re-enters the cavity. This optical feedback interferes with the intracavity field, which leads to modulation of the laser's output characteristics. These modulations are detected by a photodiode (PD) placed either in front of or behind the laser. As the target moves, its displacement induces phase shifts in the reinjected light, resulting in measurable variations in the interferometric signal.

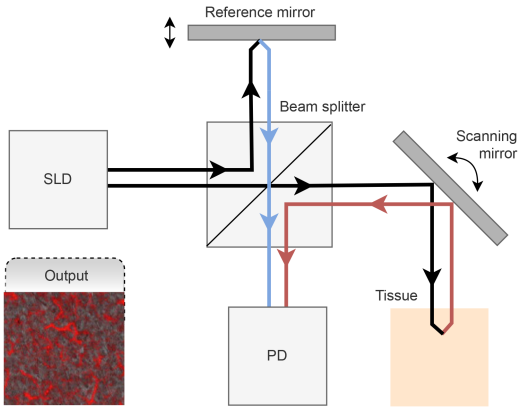

Fig. 10. Optical schematic of a time-domain OCT configuration, with the light source, beam splitter, reference and scanning mirrors and the tissue under investigation. The system measures the time delay of light backscattered from the tissue, enabling depth-resolved imaging that allows 3D imaging of the surface tissue. OCT image adapted from [199].

recombined at a sensor, creating an interference pattern from which distance information can be extracted by exploiting constructive and destructive interference. By scanning the target with an interferometer, its surface structure can be obtained at the nanometer-scale precision [187].

Self-mixing interferometry (SMI), also referred to as optical feedback interferometry (OFI), is a technique which has been introduced in the early 1980 s. In contrast to the classical interferometry, the light is not recombined in a sensor but in the laser cavity itself. The amplitude and frequency of the laser light are modulated, creating an interferometry pattern which can be measured from the laser diode voltage fluctuations, by using an internal photodiode, or by an external photodiode. The biggest advantage of SMI is that it does not need a reference optical path as the light shone onto the target is the reference. Therefore, being much simpler, this method allows for a more compact interferometry setup [96]. Configuration of SMI as well as typical SMI output are shown in Fig. 9.

SMI leverages the interference between a laser's internal field and the light reflected or scattered by moving blood cells, resulting in modulations that can be analyzed to assess blood flow dynamics. When moving blood cells reflect the laser light, their motion produces a frequency (Doppler) shift in the light fed back to the laser cavity, leading to modulation of the laser output due to interference. Analysis of the frequency or phase shifts present in the SMI output allows for quantification of blood flow parameters such as velocity, as these shifts are directly related to the speed of the moving blood cells. The foundational work has established the theoretical and instrumental basis for SMI in sensing applications [96], [188]. SMI has also shown to have potential as an alternative to conventional techniques with measuring superficial blood flow over human skin [189]. Furthermore, SMI has been shown to have an application for capturing arterial pulse waveforms by directing the laser beam at the radial artery, where reflected SMI signal enabled cardiovascular pulse shape extraction [190].

The use of laser interferometry for the characterization of bio-tissue is common in clinical settings, for dermatology or ophthalmology [98], [99]. However, they are mainly used for structural assessment of given biomarkers rather than for blood flow dynamics. Thus, SMI offers interesting prospects for dynamic microvasculature assessment [97], [191] which clinical interferometry devices do not. State-of-the art clinical interferometers are very large devices. This is mainly due to the presence of the reference optical path which is completely absent in SMI, making this technique more attractive as it allows for a more compact technology.

Recent studies suggest that SMI can be a robust, compact, and cost-effective method for non-invasive blood flow measurement [97], [192], [193], [194], [195]. The SMI is yet to be tested in microvascular monitoring.

F. Optical Coherence Tomography

Optical coherence tomography (OCT) is an imaging technique used mainly in retinal imaging, although cutaneous applications have emerged [196], [197]. Instead of highly coherent and narrow band laser light, OCT uses low-coherence light with a wide spectrum from e.g. a superluminescent diode (SLD) [198]. Sometimes called "optical ultrasound", OCT is based on the interference of low-coherence light reflecting from the tissue. The instrument is effectively a Michaelson interferometer, consisting of a light source, a photodetector, a reference mirror and a fiber optic beam splitter, splitting the light into two arms. The reference arm is directed into the reference mirror, while the measurement arm probes the tissue. The light reflected from the tissue is directed back into the device, where it interferes with the reference arm light, creating an interference pattern at the photodetector. Axial scanning in the tissue is done via moving the reference mirror towards or away from the beam splitter. Lateral scanning can be obtained by using an additional scanning mirror to the measurement arm. Optical schematic of a time-domain OCT is shown in Fig. 10. The traditional time-domain instrumentation setup has been further refined into Fourier-domain OCT [197].

Being a well-established technique in ophthalmology, most of the clinical use of OCT is related to the imaging of retinal microcirculation [196]. However, recent advances have been made in the field of cutaneous hemodynamic monitoring as well. Usage in wound healing, assessing skin cancer and the assessment of inflammatory and degenerative skin diseases have been proposed [199]. Evaluating vascular aging using reactive hyperemia exemplifies how OCT can be used to assess the skin's response to external stimuli [200]. Application of OCT in assessing CVD has primarily focused on the retinal microvasculature, but recent studies have proposed its use for cutaneous measurements as well [201]. Patients with heart failure were measured from the hand and compared with healthy subjects, showing decreased vascular density and blood flow.

Compared to MRI and ultrasound, OCT offers higher resolution, while only penetrating to approximately 0.5–1.5 mm [202].

V. Discussion and Conclusion

A recent advancement in microvasculature measurement is multimodal monitoring, where multiple techniques are combined in a single device. Miniaturized sensors make this integration possible. For example, combining spectroscopy with imaging — such as NIRS or PPG with hyperspectral imaging — offers a more comprehensive view of oxygenation and perfusion. As imaging technology and analytical algorithms improve, these multimodal methods are becoming standard in clinical practice. Multimodal methods have the potential to provide new insights through the interaction and complementarity between different data modalities.

Combining structural and functional imaging can be used to gain insights into both the static and dynamic features of the vasculature. An example of this is the combination of OCT and LSCI. OCT provides high-resolution cross-sectional images of microvascular structure, whereas LSCI captures dynamic blood flow information across the tissue surface, complementing the detailed structural data. A recent study combined multispectral imaging, retinal oximetry and LSCI to study the retinal microvasculature in the eye. The results from these modalities were combined to provide structural as well as functional information on the retina [203]. Another study used LDF, LSCI, and optical microscopy to observe the vasculature from the horizontal plane and quantify blood perfusion in wounds. In addition, fluorescence microscopy was used to reconstruct 3D vessels for longitudinal quantification. They were able to dynamically monitor angiogenesis of the wound site with this multimodal approach [204]. In another study, dynamic evaluation of microvascular blood flow has been proposed by combining LDF and high-speed nailfold videocapillaroscopy [205]. Furthermore, in endoscopic measurement combination of LSCI and PAI and combination of anti-Stoker Raman scattering, second hermonic generation and two-photon excited fluorescence have been studied [206], [207].

Machine learning is increasingly applied in optical microvascular sensing for disease risk estimation, handling large data volumes and assisting in image, and signal analysis by performing tasks such as denoising, segmenting, and feature extraction.

For example, multi-exposure LSCI, which uses multiple exposure times in contrast to traditional LSCI, generates large amounts of data, which neural networks can process. For speed-resolved perfusion imaging, that takes into account the speed distribution of blood perfusion, a neural network was trained on multi-exposure laser speckle contrast imaging data from Monte Carlo simulations of complex tissue models to estimate microcirculation and blood perfusion properties [208], [209]. LSCI has also been used to monitor blood flow and wound progression by segmenting the images using k-means clustering and computing speckle statistics to account for changes in contrast before classifying the regions to non-progressive and progressive using support vector machines [210]. In addition LSCI together with visible-light camera have been used to evaluate bowel perfusion intraoperatively using generative adversarial networks to detect ischemic regions [211].

Machine learning can also be used in disease risk estimations. Convolutional neural networks with PPG signals have been used to assess microvascular changes to estimate the risk of diabetic retinopathy [212] as well as to detect COVID-19 [42]. Furthermore, ensemble models on PPG signals have been used for cardiovascular risk detection [213]. To use microvascular imaging to monitor hemodynamics and microvascular structures or perform disease state quantification, the microvasculature needs to be segmented. This is difficult due to complex structures and low contrast. A deep learning network together with a weak signal attention mechanism and multi-scale perception model have been studied for microvasculature segmentation with photoacoustic microscopy [214]. Generative adversarial networks (GANs) have been used for unsupervised 3D segmentation of vascular networks from mesoscopic PAI in order to reduce the time-consuming and error-prone task of labeling complex tissues [215]. Unsupervised learning methods have also been used for denoising to allow microvascular visualization with low-fluence excitation using sparse coding [216].

Cutaneous measurements are desirable due to easy access to the measurement site. However, it has to be taken account that thickness of different parts of skin tissue affects also to the optical properties (foot sole vs eyelid vs breast). Additionally, cutaneous measurements are highly affected by the sympathetic nervous system making it challenging to achieve reliable and reproducible measurement. Thus, standardization of cutaneous monitoring techniques as well as algorithms are needed. Lack of standardized methods and measurements may hinder clinical adoption and reliability of presented technologies, particularly when comparing results across different devices and clinical settings.

Another important topic related to the development of instruments for diseases is responsible innovation. Although cutaneous measurement site is of interest due to its easy access, many techniques could still benefit from including other consideration related to responsible innovation [217] which encourages reflection on long-term impacts, weighing both benefits and risks. It integrates ethical, legal, and social impacts (ELSI) early in product design. Inclusion can involve diverse stakeholders—like policymakers and the public—to guide development and ensure relevance to societal needs considering e.g. utility, comfort

and cost. Such aspect were not found addressed in reviewed studies.

Many of the presented techniques here have been tested in human studies and even in clinical environments. However, large scale clinical validation studies are not conducted with most of the techniques and only few of them are in standard clinical use, leading to wide spectrum of clinical maturity of the techniques. Spectroscopic techniques NIRS and VLS are used in commercial clinical devices for tissue oxygenation evaluation, although NIRS is widely known for brain oxygenation monitoring instead of skin oxygenation monitoring. Additionally, PPG is widely used in commercial devices especially for heart rate and SpO_2 measurements, and OCT is clinically used for retinal imaging. Furthermore, there are commercial and clinically validated devices for LSCI, PAI, LDF, and microscopic techniques, especially nailfold capillaroscopy, on the market but their routine clinical use is limited. Use of DCS and SMI related to cutaneous microcirculation is still on basic research level.

We reviewed multiple techniques for cutaneous microvascular assessment and presented principles of each technique, and their clinical applications especially for cardiovascular diseases were assessed. Many of these principles overlap, providing myriad of different variants in techniques. Most of the presented techniques are still not in wide clinical use even though their clinical potential has been shown.

References

[1] C. A. Den Uil et al., "The microcirculation in health and critical disease," *Prog. Cardiovasc. Dis.*, vol. 51, no. 2, pp. 161–170, 2008.

[2] I. M. Braverman, "The cutaneous microcirculation," *J. Invest. Dermatol. Symp. Proc.*, vol. 5, no. 1, pp. 3–9, Dec. 2000.

[3] U. Aksu et al., "MicroCirculation: Current perspective in diagnostics, imaging, and clinical applications," *J. Clin. Med.*, vol. 13, no. 22, 2024, Art. no. 6762.

[4] M. Roustit and J.-L. Cracowski, "Non-invasive assessment of skin microvascular function in humans: An insight into methods," *Microcirculation*, vol. 19, no. 1, pp. 47–64, 2012.

[5] A. Lazaridis et al., "Assessing skin microcirculation in patients at cardiovascular risk by using laser speckle contrast imaging. A narrative review," *Clin. Physiol. Funct. Imag.*, vol. 43, no. 4, pp. 211–222, 2023.

[6] D. D. Gutterman et al., "The human microcirculation: Regulation of flow and beyond," *Circulation Res.*, vol. 118, no. 1, pp. 157–172, 2016.

[7] R. IJzerman et al., "Individuals at increased coronary heart disease risk are characterized by an impaired microvascular function in skin," *Eur. J. Clin. Investigation*, vol. 33, no. 7, pp. 536–542, 2003.

[8] A. Kruger et al., "Laser Doppler flowmetry detection of endothelial dysfunction in end-stage renal disease patients: Correlation with cardiovascular risk," *Kidney Int.*, vol. 70, no. 1, pp. 157–164, 2006.

[9] R. Yamamoto-Suganuma and Y. Aso, "Relationship between post-occlusive forearm skin reactive hyperaemia and vascular disease in patients with type 2 diabetes—A novel index for detecting micro-and macrovascular dysfunction using laser Doppler flowmetry," *Diabetic Med.*, vol. 26, no. 1, pp. 83–88, 2009.

[10] S. C. Agarwal et al., "Laser Doppler assessment of dermal circulatory changes in people with coronary artery disease," *Microvascular Res.*, vol. 84, no. 1, pp. 55–59, 2012.

[11] E. G. Souza et al., "Impairment of systemic microvascular endothelial and smooth muscle function in individuals with early-onset coronary artery disease: Studies with laser speckle contrast imaging," *Coronary Artery Dis.*, vol. 25, no. 1, pp. 23–28, 2014.

[12] P. A. Carberry et al., "Resting and maximal forearm skin blood flows are reduced in hypertension," *Hypertension*, vol. 20, no. 3, pp. 349–355, 1992.

[13] M. Rossi et al., "Investigation of skin vasoreactivity and blood flow oscillations in hypertensive patients: Effect of short-term antihypertensive treatment," *J. Hypertension*, vol. 29, no. 8, pp. 1569–1576, 2011.

[14] E. H. Serné et al., "Impaired skin capillary recruitment in essential hypertension is caused by both functional and structural capillary rarefaction," *Hypertension*, vol. 38, no. 2, pp. 238–242, 2001.

[15] D. Duprez et al., "Impaired microcirculation in heart failure," *Int. J. Microcirculation*, vol. 16, no. 3, pp. 137–142, 1996.

[16] J. Loader et al., "The continuums of impairment in vascular reactivity across the spectrum of cardiometabolic health: A systematic review and network meta-analysis," *Obesity Rev.*, vol. 20, no. 6, pp. 906–920, 2019.

[17] R. Rosenberry et al., "Age-related microvascular dysfunction: Novel insight from near-infrared spectroscopy," *Exp. Physiol.*, vol. 103, no. 2, pp. 190–200, Feb. 2018.

[18] E. M. Rogers et al., "Metabolic and microvascular function assessed using near-infrared spectroscopy with vascular occlusion in women: Age differences and reliability," *Exp. Physiol.*, vol. 108, no. 1, pp. 123–134, Jan. 2023.

[19] M. Horiuchi and K. Okita, "Microvascular responses during reactive hyperemia assessed by near-infrared spectroscopy and arterial stiffness in young, middle-aged, and older women," *Microvascular Res.*, vol. 129, May 2020, Art. no. 103972.

[20] R. Kragelj et al., "Parameters of postocclusive reactive hyperemia measured by near infrared spectroscopy in patients with peripheral vascular disease and in healthy volunteers," *Ann. Biomed. Eng.*, vol. 29, no. 4, pp. 311–320, Apr. 2001.

[21] D. K. Townsend et al., "Reduced insulin sensitivity in young, normoglycaemic subjects alters microvascular tissue oxygenation during postocclusive reactive hyperaemia," *Exp. Physiol.*, vol. 104, no. 6, pp. 967–974, Jun. 2019.

[22] M. P. Theodorakopoulou et al., "Muscle oxygenation and microvascular reactivity across different stages of CKD: A near-infrared spectroscopy study," *Amer. J. Kidney Dis.*, vol. 81, no. 6, pp. 655–664, Jun. 2023.

[23] J. Mesquida et al., "Peripheral microcirculatory alterations are associated with the severity of acute respiratory distress syndrome in COVID-19 patients admitted to intermediate respiratory and intensive care units," *Crit. Care*, vol. 25, no. 1, Nov. 2021, Art. no. 381.

[24] H. Schäfer et al., "Altered tissue oxygenation in patients with post COVID-19 syndrome," *Microvascular Res.*, vol. 148, Jul. 2023, Art. no. 104551.

[25] Y. Kagaya and S. Miyamoto, "A systematic review of near-infrared spectroscopy in flap monitoring: Current basic and clinical evidence and prospects," *J. Plastic, Reconstructive Aesthetic Surg.*, vol. 71, no. 2, pp. 246–257, 2018.

[26] F. F. Jöbsis, "Noninvasive, infrared monitoring of cerebral and myocardial oxygen sufficiency and circulatory parameters," *Science*, vol. 198, no. 4323, pp. 1264–1267, 1977.

[27] T. Scheeren et al., "Monitoring tissue oxygenation by near infrared spectroscopy (nirs): Background and current applications," *J. Clin. Monit. Comput.*, vol. 26, pp. 279–287, 2012.

[28] J. Mesquida et al., "Skeletal muscle oxygen saturation (STO2) measured by near-infrared spectroscopy in the critically ill patients," *BioMed Res. Int.*, vol. 2013, no. 1, 2013, Art. no. 502194.

[29] S. Jones et al., "Recent developments in near-infrared spectroscopy (NIRS) for the assessment of local skeletal muscle microvascular function and capacity to utilise oxygen," *Artery Res.*, vol. 16, pp. 25–33, 2016.

[30] M. Shaaban-Ali et al., "Clinical and technical limitations of cerebral and somatic near-infrared spectroscopy as an oxygenation monitor," *J. Cardiothoracic Vasc. Anesth.*, vol. 35, no. 3, pp. 763–779, Mar. 2021.

[31] R. J. Cooper et al., "A systematic comparison of motion artifact correction techniques for functional near-infrared spectroscopy," *Front. Neurosci.*, vol. 6, 2012, Art. no. 147.

[32] G. A. Murphy et al., "Quantifying dermal microcirculatory changes of neuropathic and neuroischemic diabetic foot ulcers using spatial frequency domain imaging: A shade of things to come," *BMJ Open Diabetes Res. Care*, vol. 8, no. 2, Nov. 2020, Art. no. e001815.

[33] L. Urbanavičius et al., "How to assess intestinal viability during surgery: A review of techniques," *World J. Gastrointestinal Surg.*, vol. 3, no. 5, pp. 59–69, 2011.

[34] A. Karliczek et al., "Intraoperative assessment of microperfusion with visible light spectroscopy for prediction of anastomotic leakage in colorectal anastomoses," *Colorectal Dis.*, vol. 12, no. 10, pp. 1018–1025, 2010.

[35] D. A. Benaron et al., "Design of a visible-light spectroscopy clinical tissue oximeter," *J. Biomed. Opt.*, vol. 10, no. 4, 2005, Art. no. 044005.

[36] D. A. Benaron et al., "Continuous, noninvasive, and localized microvascular tissue oximetry using visible light spectroscopy," *Anesthesiol.*, vol. 100, no. 6, pp. 1469–1475, 2004.

[37] J. Allen and A. Murray, "Age-related changes in the characteristics of the photoplethysmographic pulse shape at various body sites," *Physiol. Meas.*, vol. 24, no. 2, pp. 297–307, May 2003.

[38] Y. Hu et al., "Comparative study of photoplethysmographic waveforms with application of antihypertensive medication in hypertensive patients," *Ann. Noninvasive Electrocardiol.*, vol. 27, no. 3, May 2022, Art. no. e12941.

[39] K. Bogusz-Górna et al., "Non-invasive detection of early microvascular changes in juveniles with type 1 diabetes," *Cardiovasc. Diabetol.*, vol. 22, no. 1, 2023, Art. no. 285.

[40] G. Horstick et al., "Tissue optical perfusion pressure: A simplified, more reliable, and faster assessment of pedal microcirculation in peripheral artery disease," *Amer. J. Physiol. Heart Circulatory Physiol.*, vol. 319, no. 6, pp. H1208–H1220, Dec. 2020.

[41] P.-C. Hsu et al., "Assessment of subtle changes in diabetes-associated arteriosclerosis using photoplethysmographic pulse wave from index finger," *J. Med. Syst.*, vol. 42, no. 3, Jan. 2018, Art. no. 43.

[42] S. Lombardi et al., "COVID-19 detection using photoplethysmography and neural networks," *Sensors*, vol. 23, no. 5, Feb. 2023, Art. no. 2561.

[43] E. Rossi et al., "COVID-19 detection using a model of photoplethysmography (PPG) signals," *Med. Eng. Phys.*, vol. 109, Nov. 2022, Art. no. 103904.

[44] Y. Sun and N. Thakor, "Photoplethysmography revisited: From contact to noncontact, from point to imaging," *IEEE Trans. Biomed. Eng.*, vol. 63, no. 3, pp. 463–477, Mar. 2016.

[45] J.-P. Sirkiä et al., "Multi-wavelength photoplethysmography device for the measurement of pulse transit time in the skin microvasculature," in *Proc. 2020 Comput. Cardiol.*, 2020, pp. 1–4.

[46] J. Allen, "Photoplethysmography and its application in clinical physiological measurement," *Physiol. Meas.*, vol. 28, p. R1-39, Apr. 2007, doi: 10.1088/0967-3334/28/3/R01.

[47] S. Premkumar and D. J. Hemanth, "Intelligent remote photoplethysmography-based methods for heart rate estimation from face videos: A survey," *Informatics*, vol. 9, no. 3, Sep. 2022, Art. no. 57.

[48] P. V. Rouast et al., "Remote heart rate measurement using low-cost RGB face video: A technical literature review," *Front. Comput. Sci.*, vol. 12, no. 5, pp. 858–872, Oct. 2018.

[49] S. Chatterjee et al., "Investigating the origin of photoplethysmography using a multiwavelength Monte Carlo model," *Physiol. Meas.*, vol. 41, no. 8, 2020, Art. no. 84001.

[50] B. J. Sumpio et al., "Use of hyperspectral imaging to assess endothelial dysfunction in peripheral arterial disease," *J. Vasc. Surg.*, vol. 64, no. 4, pp. 1066–1073, Oct. 2016.

[51] J. A. Chin et al., "Evaluation of hyperspectral technology for assessing the presence and severity of peripheral artery disease," *J. Vasc. Surg.*, vol. 54, no. 6, pp. 1679–1688, Dec. 2011.

[52] N. Chiang et al., "Evaluation of hyperspectral imaging technology in patients with peripheral vascular disease," *J. Vasc. Surg.*, vol. 66, no. 4, pp. 1192–1201, Oct. 2017.

[53] R. L. Greenman et al., "Early changes in the skin microcirculation and muscle metabolism of the diabetic foot," *Lancet*, vol. 366, no. 9498, pp. 1711–1717, Nov. 2005.

[54] L. Khaodhiar et al., "The use of medical hyperspectral technology to evaluate microcirculatory changes in diabetic foot ulcers and to predict clinical outcomes," *Diabetes Care*, vol. 30, no. 4, pp. 903–910, Apr. 2007.

[55] D. Yudovsky et al., "Assessing diabetic foot ulcer development risk with hyperspectral tissue oximetry," *J. Biomed. Opt.*, vol. 16, no. 2, Feb. 2011, Art. no. 026009.

[56] A. Nouvong et al., "Evaluation of diabetic foot ulcer healing with hyperspectral imaging of oxyhemoglobin and deoxyhemoglobin," *Diabetes Care*, vol. 32, no. 11, pp. 2056–2061, Jul. 2009.

[57] E. L. P. Larsen et al., "Hyperspectral imaging of atherosclerotic plaques in vitro," *J. Biomed. Opt.*, vol. 16, no. 2, Feb. 2011, Art. no. 026011.

[58] A. A. Lindelauf et al., "Near-infrared spectroscopy (NIRS) versus hyperspectral imaging (HSI) to detect flap failure in reconstructive surgery: A systematic review," *Life*, vol. 12, no. 1, 2022, Art. no. 65.

[59] G. Lu and B. Fei, "Medical hyperspectral imaging: A review," *Proc. SPIE*, vol. 19, no. 1, 2014, Art. no. 010901.

[60] M. López-Moral et al., "A comparison of hyperspectral imaging with routine vascular noninvasive techniques to assess the healing prognosis in patients with diabetic foot ulcers," *J. Vasc. Surg.*, vol. 75, no. 1, pp. 255–261, 2022.

[61] O. Hart et al., "The utility of hyperspectral imaging in patients with chronic venous disorders," *J. Vasc. Surgery, Venous Lymphat. Disord.*, vol. 10, no. 6, pp. 1325–1333, 2022.

[62] W. Groner et al., "Orthogonal polarization spectral imaging: A new method for study of the microcirculation," *Nature Med.*, vol. 5, no. 10, pp. 1209–1212, Oct. 1999.

[63] V. Cerný et al., "Orthogonal polarization spectral imaging," *Physiol. Res.*, vol. 56, no. 2, pp. 141–147, 2007.

[64] P. T. Goedhart et al., "Sidestream dark field (SDF) imaging: A novel stroboscopic LED ring-based imaging modality for clinical assessment of the microcirculation," *Opt. Exp.*, vol. 15, no. 23, pp. 15101–15114, Nov. 2007.

[65] H. Sherman et al., "Incident dark-field illumination: A new method for microcirculatory study," *Angiology*, vol. 22, no. 5, pp. 295–303, May 1971.

[66] T. Reynolds et al., "Observational study of the effects of age, diabetes mellitus, cirrhosis and chronic kidney disease on sublingual microvascular flow," *Crit. Care*, vol. 17, pp. 1–200, 2013.

[67] V. Smith et al., "Nailfold capillaroscopy," *Best Pract. Res. Clin. Rheumatol.*, vol. 37, no. 1, 2023, Art. no. 101849.

[68] P. Vuilleumier et al., "Postischemic forearm skin reactive hyperemia is related to cardovascular risk factors in a healthy female population," *J. Hypertension*, vol. 20, no. 9, pp. 1753–1757, Sep. 2002.

[69] M. Rossi et al., "Peripheral microvascular dysfunction as an independent predictor of atherosclerotic damage in type 1 diabetes patients: A preliminary study," *Clin. Hemorheol. Microcirculation*, vol. 54, no. 4, pp. 381–391, 2013.

[70] R. Yamamoto-Suganuma and Y. Aso, "Relationship between post-occlusive forearm skin reactive hyperaemia and vascular disease in patients with type 2 diabetes–A novel index for detecting micro- and macrovascular dysfunction using laser Doppler flowmetry," *Diabetic Med., J. Brit. Diabetic Assoc.*, vol. 26, no. 1, pp. 83–88, Jan. 2009.

[71] I. Cordovil et al., "Evaluation of systemic microvascular endothelial function using laser speckle contrast imaging," *Microvascular Res.*, vol. 83, no. 3, pp. 376–379, May 2012.

[72] M.-E. Alexandrou et al., "Haemodialysis and peritoneal dialysis patients have severely impaired post-occlusive skin forearm vasodilatory response assessed with laser speckle contrast imaging," *Clin. Kidney J.*, vol. 14, no. 5, pp. 1419–1427, 2021.

[73] A. Lazaridis et al., "Skin microvascular function, as assessed with laser speckle contrast imaging, is impaired in untreated essential and masked hypertension," *Hypertension Res.*, vol. 45, no. 3, pp. 445–454, Mar. 2022.

[74] A. S. De Matheus et al., "Assessment of microvascular endothelial function in type 1 diabetes using laser speckle contrast imaging," *J. Diabetes Complications*, vol. 31, no. 4, pp. 753–757, Apr. 2017.

[75] J. Borges et al., "A novel effective method for the assessment of microvascular function in male patients with coronary artery disease: A pilot study using laser speckle contrast imaging," *Braz. J. Med. Biol. Res.*, vol. 49, no. 10, Sep. 2016, Art. no. e5541.

[76] J. P. Borges et al., "The impact of exercise frequency upon microvascular endothelium function and oxidative stress among patients with coronary artery disease," *Clin. Physiol. Funct. Imag.*, vol. 38, no. 5, pp. 840–846, Sep. 2018.

[77] M. A. Davis et al., "Imaging depth and multiple scattering in laser speckle contrast imaging," *J. Biomed. Opt.*, vol. 19, no. 8, pp. 086001–086001, 2014.

[78] J. Senarathna et al., "Laser speckle contrast imaging: Theory, instrumentation and applications," *IEEE Rev. Biomed. Eng.*, vol. 6, pp. 99–110, 2013.

[79] D. Briers et al., "Laser speckle contrast imaging: Theoretical and practical limitations," *Proc. SPIE*, vol. 18, no. 6, 2013, Art. no. 066018.

[80] A. Rege et al., "Imaging microvascular flow characteristics using laser speckle contrast imaging," in *Proc. Annu. Int. Conf. IEEE Eng. Med. Biol.*, 2010, pp. 1978–1981.

[81] S. A. Carp et al., "Diffuse correlation spectroscopy: Current status and future outlook," *Proc. SPIE*, vol. 10, no. 1, 2023, Art. no. 013509.

[82] T. Durduran et al., "Diffuse optics for tissue monitoring and tomography," *Rep. Prog. Phys.*, vol. 73, no. 7, 2010, Art. no. 076701.

[83] D. A. Boas et al., "Establishing the diffuse correlation spectroscopy signal relationship with blood flow," *Neurophotonics*, vol. 3, no. 3, Jun. 2016, Art. no. 031412.

[84] E. James and P. R. Munro, "Diffuse correlation spectroscopy: A review of recent advances in parallelisation and depth discrimination techniques," *Sensors*, vol. 23, no. 23, 2023, Art. no. 9338.

[85] G. Yu, "Diffuse correlation spectroscopy (DCS): A diagnostic tool for assessing tissue blood flow in vascular-related diseases and therapies," *Curr. Med. Imag. Rev.*, vol. 8, no. 3, pp. 194–210, 2012.

[86] K. Mizukoshi et al., "Quantitative analysis of age-related changes in vascular structure, oxygen saturation, and epidermal melanin structure using photoacoustic methods," *Skin Res. Technol.*, vol. 30, no. 1, 2024, Art. no. e13537.

[87] A. Karlas et al., "Cardiovascular optoacoustics: From mice to men–A review," *Photoacoustics*, vol. 14, pp. 19–30, 2019.

[88] L. Lin and L. V. Wang, "The emerging role of photoacoustic imaging in clinical oncology," *Nature Rev. Clin. Oncol.*, vol. 19, no. 6, pp. 365–384, 2022.

[89] J. Yang et al., "Detecting hemodynamic changes in the foot vessels of diabetic patients by photoacoustic tomography," *J. Biophotonics*, vol. 13, no. 8, 2020, Art. no. 0202000011.

[90] A. Karlas et al., "Dermal features derived from optoacoustic tomograms via machine learning correlate microangiopathy phenotypes with diabetes stage," *Nature Biomed. Eng.*, vol. 7, no. 12, pp. 1667–1682, 2023.

[91] S. Mirg et al., "Photoacoustic imaging for microcirculation," *Microcirculation*, vol. 29, no. 6/7, 2022, Art. no. e12776.

[92] A. B. E. Attia et al., "A review of clinical photoacoustic imaging: Current and future trends," *Photoacoustics*, vol. 16, 2019, Art. no. 100144.

[93] I. Steinberg et al., "Photoacoustic clinical imaging," *Photoacoustics*, vol. 14, pp. 77–98, 2019.

[94] K. Farkas et al., "Non-invasive assessment of microvascular endothelial function by laser Doppler flowmetry in patients with essential hypertension," *Atherosclerosis*, vol. 173, no. 1, pp. 97–102, 2004.

[95] T. Ishii et al., "Laser Doppler blood flowmeter as a useful instrument for the early detection of lower extremity peripheral arterial disease in hemodialysis patients: An observational study," *BMC Nephrol.*, vol. 20, no. 1, 2019, Art. no. 470.

[96] S. Donati, "Developing self-mixing interferometry for instrumentation and measurements," *Laser Photon. Rev.*, vol. 6, no. 3, pp. 393–417, 2012.

[97] A. Quotb et al., "Methods and limits for micro scale blood vessel flow imaging in scattering media by optical feedback interferometry: Application to human skin," *Sensors*, vol. 21, no. 4, 2021, Art. no. 1300.

[98] E. Sattler et al., "Optical coherence tomography in dermatology," *J. Biomed. Opt.*, vol. 18, Jun. 2013, Art. no. 061224.

[99] M. Zeppieri et al., "Optical coherence tomography (OCT): A brief look at the uses and technological evolution of ophthalmology," *Medicina (Kaunas)*, vol. 59, Dec. 2023, Art. no. 2114.

[100] M. F. Yang, V. V. Tuchin, and A. N. Yaroslavsky, "Principles of light-skin interactions," in *Light-Based Therapies for Skin of Color*, E. Baron, Ed. London, U.K.: Springer, 2009, pp. 1–44.

[101] W. Wang et al., "Algorithmic principles of remote PPG," *IEEE Trans. Biomed. Eng.*, vol. 64, no. 7, pp. 1479–1491, Jul. 2017.

[102] E. Austin et al., "Visible light. Part I: Properties and cutaneous effects of visible light," *J. Amer. Acad. Dermatol.*, vol. 84, no. 5, pp. 1219–1231, May 2021.

[103] T. Lister et al., "Optical properties of human skin," *J. Biomed. Opt.*, vol. 17, no. 9, Sep. 2012, Art. no. 090901.

[104] P. Beard, "Biomedical photoacoustic imaging," *Interface Focus*, vol. 1, no. 4, pp. 602–631, 2011.

[105] C. Mignon et al., "Shedding light on the variability of optical skin properties: Finding a path towards more accurate prediction of light propagation in human cutaneous compartments," *Biomed. Opt. Exp.*, vol. 9, no. 2, pp. 852–872, Feb. 2018.

[106] L. Finlayson et al., "Depth penetration of light into skin as a function of wavelength from 200 to 1000 nm," *Photochemistry Photobiol.*, vol. 98, no. 4, pp. 974–981, 2022.

[107] S. L. Jacques, "Simple theory, measurements, and rules of thumb for dosimetry during photodynamic therapy," *Proc SPIE*, vol. 1065, pp. 100–108, 1989, doi: 10.1117/12.978009.

[108] J.-P. Sirkiä et al., "Tonometric multi-wavelength photoplethysmography for studying the cutaneous microvasculature of the fingertip," *IEEE Trans. Instrum. Meas.*, vol. 72, 2023, Art. no. 4009113.

[109] J.-P. Sirkiä et al., "Non-invasive hemodynamic monitoring system integrating spectrometry, photoplethysmography, and arterial pressure measurement capabilities," *Adv. Sci.*, vol. 11, no. 24, 2024, Art. no. 2310022.

[110] A. Chandrasekhar et al., "PPG sensor contact pressure should be taken into account for cuff-less blood pressure measurement," *IEEE Trans. Biomed. Eng.*, vol. 67, no. 11, pp. 3134–3140, Nov. 2020.

[111] S. L. Jacques, "Tutorial on monte carlo simulation of photon transport in biological tissues," *Biomed. Opt. Exp.*, vol. 14, no. 2, pp. 559–576, 2023.

[112] S. A. Prahl et al., "A Monte Carlo model of light propagation in tissue," *Proc. SPIE*, vol. 10305, pp. 105–114, 1989.

[113] F. Syed et al., "Modeling dynamics of the cardiovascular system using fluid-structure interaction methods," *Biology*, vol. 12, no. 7, 2023, Art. no. 1026.

[114] M. Sarkar and M. Assaad, "Noninvasive non-contact SPO2 monitoring using an integrated polarization-sensing CMOs imaging sensor," *Sensors*, vol. 22, no. 20, 2022, Art. no. 7796.

[115] J. E. Sinex, "Pulse oximetry: Principles and limitations," *Amer. J. Emerg. Med.*, vol. 17, no. 1, pp. 59–66, 1999.

[116] T. Barker et al., "An evaluation of the normal range of sto2 measurements at rest and following a mixed exercise protocol," *BMJ Mil. Health*, vol. 161, no. 4, pp. 327–331, 2015.

[117] B. A. Crookes et al., "Can near-infrared spectroscopy identify the severity of shock in trauma patients?," *J. Trauma Acute Care Surg.*, vol. 58, no. 4, pp. 806–816, 2005.

[118] M. Holmes et al., "Aging alters gastrocnemius muscle hemoglobin oxygen saturation (STO2) characteristics in healthy individuals," *Eur. J. Appl. Physiol.*, vol. 122, no. 6, pp. 1509–1520, 2022.

[119] A. J. Comerota et al., "Tissue (muscle) oxygen saturation (STO2): A new measure of symptomatic lower-extremity arterial disease," *J. Vasc. Surg.*, vol. 38, no. 4, pp. 724–729, 2003.

[120] D. A. Benaron et al., "Quantitative clinical nonpulsatile and localized visible light oximeter: Design of the T-stat tissue oximeter," *Proc. SPIE*, vol. 4955, pp. 355–368, 2003.

[121] M. H. Niemz, *Laser-Tissue Interactions : Fundamentals and Applications* (Biological and Medical Physics, Biomedical Engineering Series), 3rd ed. Berlin, Germany: Springer, 2007.

[122] M. F. Yang et al., "Principles of light-skin interactions," in *Proc. Light-Based Therapies Skin Color*. London, U.K.: Springer 2009, pp. 1–44.

[123] J. M. Smit et al., "Advancements in free flap monitoring in the last decade: A critical review," *Plast. Reconstructive Surg.*, vol. 125, no. 1, p. 177–185, 2010.

[124] S. P. Moubayed et al., "What are the optimal monitoring techniques in head and neck microvascular reconstruction?," *Orl*, vol. 78, no. 5, pp. 241–244, 2016.

[125] K. Zaleski et al., "Does sex influence near-infrared spectroscopy-derived indicators of microvascular reactivity and the response to acute dietary capsaicin," *Microvascular Res.*, vol. 145, Jan. 2023, Art. no. 104436.

[126] K. B. Kim and H. J. Baek, "Photoplethysmography in wearable devices: A comprehensive review of technological advances, current challenges, and future directions," *Electronics*, vol. 12, no. 13, 2023, Art. no. 2923.

[127] B. A. Fallow et al., "Influence of skin type and wavelength on light wave reflectance," *J. Clin. Monit. Comput.*, vol. 27, pp. 313–317, 2013.

[128] Y. Maeda et al., "Comparison of reflected green light and infrared photoplethysmography," in *Proc. 30th Annu. Int. Conf. IEEE Eng. Med. Biol. Soc.*, 2008, pp. 2270–2272.

[129] J. Yao and S. Warren, "A novel algorithm to separate motion artifacts from photoplethysmographic signals obtained with a reflectance pulse oximeter," in *Proc. 26th Annu. Int. Conf. IEEE Eng. Med. Biol. Soc.*, 2004, vol. 1, pp. 2153–2156.

[130] D. Ray et al., "A review of wearable multi-wavelength photoplethysmography," *IEEE Rev. Biomed. Eng.*, vol. 16, pp. 136–151, 2023.

[131] Z. Ovadia-Blechman et al., "Peripheral microcirculatory hemodynamic changes in patients with myocardial ischemia," *Biomed. Pharmacother.*, vol. 74, pp. 83–88, Aug. 2015.

[132] A. Saglietto et al., "Beat-to-beat finger photoplethysmography in atrial fibrillation patients undergoing electrical cardioversion," *Sci. Rep.*, vol. 13, no. 1, Apr. 2023, Art. no. 6751.

[133] A. Al-Naji et al., "Monitoring of cardiorespiratory signal: Principles of remote measurements and review of methods," *IEEE Access*, vol. 5, pp. 15776–15790, 2017.

[134] P.-W. Huang et al., "A heart rate monitoring framework for real-world drivers using remote photoplethysmography," *IEEE J. Biomed. Health Inform.*, vol. 25, no. 5, pp. 1397–1408, May 2021.

[135] J.-C. Cobos-Torres et al., "Non-contact, simple neonatal monitoring by photoplethysmography," *Sensors*, vol. 18, no. 12, Dec. 2018, Art. no. 4362.

[136] S. Zaunseder et al., "Cardiovascular assessment by imaging photoplethysmography–a review," *Biomed. Eng. / Biomedizinische Technik*, vol. 63, no. 5, pp. 617–634, Oct. 2018.

[137] D. McDuff et al., "Improvements in remote cardiopulmonary measurement using a five band digital camera," *IEEE Trans. Biomed. Eng.*, vol. 61, no. 10, pp. 2593–2601, Oct. 2014.

[138] M. van Gastel et al., "Motion robust remote-PPG in infrared," *IEEE Trans. Biomed. Eng.*, vol. 62, no. 5, pp. 1425–1433, May 2015.

[139] M. J. Bautista et al., "Clinical applications of contactless photoplethysmography for monitoring in adults: A systematic review and meta-analysis," *J. Clin. Transl. Sci.*, vol. 7, no. 1, Jan. 2023, Art. no. e129.

[140] E. Grambow et al., "Hyperspectral imaging for monitoring of perfusion failure upon microvascular anastomosis in the rat hind limb," *Microvascular Res.*, vol. 116, pp. 64–70, 2018.

[141] I. Gurov et al., "High-speed video capillaroscopy method for imaging and evaluation of moving red blood cells," *Opt. Lasers Eng.*, vol. 104, pp. 244–251, 2018.

[142] G. Maldonado et al., "Nailfold capillaroscopy in diabetes mellitus," *Microvascular Res.*, vol. 112, pp. 41–46, 2017.

[143] S. Yüksel et al., "Abnormal nailfold videocapillaroscopic findings in heart failure patients with preserved ejection fraction," *Clin. Hemorheol. Microcirculation*, vol. 77, no. 1, pp. 115–121, 2021.

[144] M. W. Lim et al., "Nailfold video-capillaroscopy in the study of cardiovascular disease: A systematic review," *Blood Press. Monit.*, vol. 28, no. 1, pp. 24–32, 2023.

[145] O. Genzel-Boroviczény et al., "Orthogonal polarization spectral imaging (OPS): A novel method to measure the microcirculation in term and preterm infants transcutaneously," *Pediatr. Res.*, vol. 51, no. 3, pp. 386–391, 2002.

[146] D. A. Bottino and E. Bouskela, "Non-invasive techniques to access in vivo the skin microcirculation in patients," *Front. Med.*, vol. 9, 2023, Art. no. 1099107.

[147] J. A. Fan et al., "Near-normal incidence dark-field microscopy: Applications to nanoplasmonic spectroscopy," *Nano Lett.*, vol. 12, no. 6, pp. 2817–2821, 2012.

[148] H. Van Elteren et al., "Cutaneous microcirculation in preterm neonates: Comparison between sidestream dark field (SDF) and incident dark field (IDF) imaging," *J. Clin. Monit. Comput.*, vol. 29, pp. 543–548, 2015.

[149] N. Golubova et al., "Time–frequency analysis of laser speckle contrast for transcranial assessment of cerebral blood flow," *Biomed. Signal Process. Control*, vol. 85, 2023, Art. no. 104969.

[150] I. Mizeva et al., "Wavelet analysis of the temporal dynamics of the laser speckle contrast in human skin," *IEEE Trans. Biomed. Eng.*, vol. 67, no. 7, pp. 1882–1889, Jul. 2020.

[151] M.-C. Hsieh et al., "Noncontact monitoring of the peripheral microcirculation using laser speckle contrast imaging to evaluate the skin perfusion pressure," *Results Eng.*, vol. 26, 2025, Art. no. 105528.

[152] M.-C. Hsieh et al., "Comprehensive validation of a compact laser speckle contrast imaging system for vascular function assessment: From the laboratory to the clinic," *Med. Biol. Eng. Comput.*, vol. 63, no. 3, pp. 641–659, 2025.

[153] M. Ghijsen et al., "Wearable speckle plethysmography (SPG) for characterizing microvascular flow and resistance," *Biomed. Opt. Exp.*, vol. 9, no. 8, pp. 3937–3952, 2018.

[154] J. H. Olazábal et al., "Beat-to-beat intervals of speckle & intensity-based optical plethysmograms compared to electrocardiogram," in *Proc. Comput. Cardiol.*, 2021, vol. 48, pp. 1–4.

[155] J. H. Olazábal et al., "Camera-derived photoplethysmography (RPPG) and speckle plethysmography (RSPG): Comparing reflective and transmissive mode at various integration times using leds and lasers," *Sensors*, vol. 22, no. 16, 2022, Art. no. 6059.

[156] J. H. Olazabal et al., "Comparison between speckle plethysmography and photoplethysmography during cold pressor test referenced to finger arterial pressure," *Sensors*, vol. 23, no. 11, 2023, Art. no. 5016.

[157] J. H. Olazabal et al., "Comparing remote speckle plethysmography and finger-CLIP photoplethysmography with non-invasive finger arterial pressure pulse waves, regarding morphology and arrival time," *Bioengineering*, vol. 10, no. 1, 2023, Art. no. 101.

[158] H. Ayaz et al., "Optical imaging and spectroscopy for the study of the human brain: Status report," *Neurophotonics*, vol. 9, no. S2, 2022, Art. no. S24001.

[159] Q. Wang et al., "A comprehensive overview of diffuse correlation spectroscopy: Theoretical framework, recent advances in hardware, analysis, and applications," *NeuroImage*, vol. 298, 2024, Art. no. 120793.

[160] S. A. Carp et al., "Validation of diffuse correlation spectroscopy measurements of rodent cerebral blood flow with simultaneous arterial spin labeling MRI; towards MRI-optical continuous cerebral metabolic monitoring," *Biomed. Opt. Exp.*, vol. 1, no. 2, pp. 553–565, 2010.

[161] E. M. Buckley et al., "Cerebral hemodynamics in preterm infants during positional intervention measured with diffuse correlation spectroscopy and transcranial Doppler ultrasound," *Opt. Exp.*, vol. 17, no. 15, pp. 12571–12581, 2009.

[162] D. Grosenick et al., "Review of optical breast imaging and spectroscopy," *Proc. SPIE*, vol. 21, no. 9, 2016, Art. no. 091311.

[163] H. S. Yazdi et al., "Mapping breast cancer blood flow index, composition, and metabolism in a human subject using combined diffuse optical spectroscopic imaging and diffuse correlation spectroscopy," *Proc. SPIE*, vol. 22, no. 4, 2017, Art. no. 045003.

[164] Y. Shang et al., "Diffuse correlation spectroscopy (DCS) for assessment of tissue blood flow in skeletal muscle: Recent progress," *Anatomy Physiol., Curr. Res.*, vol. 3, no. 2, p. 128, Dec. 2013, doi: 10.4172/2161-0940.1000128.

[165] V. Quaresima et al., "Diffuse correlation spectroscopy and frequency-domain near-infrared spectroscopy for measuring microvascular blood flow in dynamically exercising human muscles," *J. Appl. Physiol.*, vol. 127, no. 5, pp. 1328–1337, 2019.

[166] E. Sathialingam et al., "Small separation diffuse correlation spectroscopy for measurement of cerebral blood flow in rodents," *Biomed. Opt. Exp.*, vol. 9, no. 11, pp. 5719–5734, 2018.

[167] B. Rinehart et al., "Quantification of perfusion and metabolism in an autism mouse model assessed by diffuse correlation spectroscopy and near-infrared spectroscopy," *J. Biophotonics*, vol. 14, no. 11, 2021, Art. no. e202000454.

[168] C. Huang et al., "Speckle contrast diffuse correlation tomography of cerebral blood flow in perinatal disease model of neonatal piglets," *J. Biophotonics*, vol. 14, no. 4, 2021, Art. no. e202000366.

[169] W. J. Tucker et al., "Studies into the determinants of skeletal muscle oxygen consumption: Novel insight from near-infrared diffuse correlation spectroscopy," *J. Physiol.*, vol. 597, no. 11, pp. 2887–2901, Jun. 2019.

[170] Y.-S. Chen et al., "Chapter 9 - photoacoustic imaging for Cancer diagnosis and therapy guidance," in *Cancer Theranostics*, X. Chen and S. Wong, Eds. Oxford, U.K.: Academic Press, 2014, pp. 139–158.

[171] Y. Wang et al., "Compressed sensing for biomedical photoacoustic imaging: A review," *Sensors*, vol. 24, no. 9, 2024, Art. no. 2670.

[172] N. Huynh et al., "A fast all-optical 3D photoacoustic scanner for clinical vascular imaging," *Nature Biomed. Eng.*, vol. 9, no. 5, pp. 638–655, 2025.

[173] Y. Zhang et al., "Ultrafast longitudinal imaging of haemodynamics via single-shot volumetric photoacoustic tomography with a single-element detector," *Nature Biomed. Eng.*, vol. 8, no. 6, pp. 712–725, 2024.

[174] S. Na et al., "Massively parallel functional photoacoustic computed tomography of the human brain," *Nature Biomed. Eng.*, vol. 6, no. 5, pp. 584–592, 2022.

[175] C. Liu and L. Wang, "Functional photoacoustic microscopy of hemodynamics: A review," *Biomed. Eng. Lett.*, vol. 12, no. 2, pp. 97–124, 2022.

[176] M. Masthoff et al., "Multispectral optoacoustic tomography of systemic sclerosis," *J. Biophotonics*, vol. 11, no. 11, 2018, Art. no. e201800155.

[177] M. Masthoff et al., "Use of multispectral optoacoustic tomography to diagnose vascular malformations," *JAMA Dermatol.*, vol. 154, no. 12, pp. 1457–1462, 2018.

[178] J. R. Eisenbrey et al., "Photoacoustic oxygenation quantification in patients with Raynaud's: First-in-human results," *Ultrasound Med. Biol.*, vol. 44, no. 10, pp. 2081–2088, 2018.

[179] A. P. Shepherd and P. Å. Öberg, *Laser-Doppler Blood Flowmetry*, vol. 107. New York, NY, USA: Springer Science & Business Media, 2013.

[180] I. Fredriksson et al., "Measurement depth and volume in laser Doppler flowmetry," *Microvascular Res.*, vol. 78, no. 1, pp. 4–13, Jun. 2009.

[181] A. M. Seifalian et al., "Comparison of laser Doppler perfusion imaging, laser Doppler flowmetry, and thermographic imaging for assessment of blood flow in human skin," *Eur. J. Vasc. Surg.*, vol. 8, no. 1, pp. 65–69, Jan. 1994.

[182] T. Binzoni et al., "Non-invasive laser Doppler perfusion measurements of large tissue volumes and human skeletal muscle blood RMS velocity," *Phys. Med. Biol.*, vol. 48, no. 15, 2003, Art. no. 2527.

[183] V. Rajan et al., "Review of methodological developments in laser Doppler flowmetry," *Lasers Med. Sci.*, vol. 24, pp. 269–283, 2009.

[184] Z. Girkantaite et al., "Laser Doppler flowmetry evaluation of skin microvascular endothelial function in patients with metabolic syndrome," *Microvascular Res.*, vol. 142, 2022, Art. no. 104373.

[185] M. Tezuka et al., "Feasibility of portable laser Doppler flowmeter for foot blood flow assessment in patients with chronic limb threatening ischaemia," *EJVES Vasc. Forum*, vol. 64, pp. 166–173, 2025.

[186] S. Willems et al., "Description of peripheral blood perfusion by laser speckle contrast analysis (LASCA) in 'early' versus 'clinically overt' systemic sclerosis in routine clinics," *Diagnostics*, vol. 13, no. 9, 2023, Art. no. 1566.
[187] D. D. Nolte, *Optical Interferometry for Biology and Medicine*, vol. 1. New York, NY, USA: Springer Science & Business Media, 2012.
[188] G. Giuliani et al., "Laser diode self-mixing technique for sensing applications," *J. Opt., Pure Appl. Opt.*, vol. 4, no. 6, 2002, Art. no. S283.
[189] S. K. Ozdemir et al., "Self-mixing laser speckle velocimeter for blood flow measurement," *IEEE Trans. Instrum. Meas.*, vol. 49, no. 5, pp. 1029–1035, Oct. 2000.
[190] J. Hast et al., "Arterial pulse shape measurement using self-mixing effect in a diode laser," *Quantum Electron.*, vol. 32, no. 11, 2002, Art. no. 975.
[191] E. E. Ramírez Miquet et al., "Optical feedback interferometry: From basics to applications of laser flowmetry," *Revista Cubana de Fıśica*, vol. 34, pp. 48–57, Jul. 2017.
[192] M. Norgia et al., "Low-cost optical flowmeter with analog front-end electronics for blood extracorporeal circulators," *IEEE Trans. Instrum. Meas.*, vol. 59, no. 5, pp. 1233–1239, May 2010.
[193] M. Norgia et al., "Self-mixing laser Doppler spectra of extracorporeal blood flow: A theoretical and experimental study," *IEEE Sensors J.*, vol. 12, no. 3, pp. 552–557, Mar. 2012.
[194] L. Campagnolo et al., "A new optical feedback interferometer for measuring red blood cell velocity distributions in individual capillaries: A feasibility study in microchannels," *Comput. Methods Biomech. Biomed. Eng.*, vol. 15, no. sup1, pp. 104–105, 2012.
[195] L. Campagnolo et al., "Flow profile measurement in microchannel using the optical feedback interferometry sensing technique," *Microfluidics Nanofluidics*, vol. 14, no. 1, pp. 113–119, 2013.
[196] D. Thomas and G. Duguid, "Optical coherence tomography—A review of the principles and contemporary uses in retinal investigation," *Eye*, vol. 18, no. 6, pp. 561–570, 2004.
[197] R. Leitgeb et al., "Performance of fourier domain vs. time domain optical coherence tomography," *Opt. Exp.*, vol. 11, no. 8, pp. 889–894, 2003.
[198] D. Huang et al., "Optical coherence tomography," *Science*, vol. 254, no. 5035, pp. 1178–1181, 1991.
[199] S. Schuh et al., "Imaging blood vessel morphology in skin: Dynamic optical coherence tomography as a novel potential diagnostic tool in dermatology," *Dermatol. Ther.*, vol. 7, pp. 187–202, 2017.
[200] M. Wang-Evers et al., "Assessing the impact of aging and blood pressure on dermal microvasculature by reactive hyperemia optical coherence tomography angiography," *Sci. Rep.*, vol. 11, no. 1, 2021, Art. no. 13411.
[201] D. F. Sciarrone et al., "Visualising and quantifying microvascular structure and function in patients with heart failure using optical coherence tomography," *J. Physiol.*, vol. 600, no. 17, pp. 3921–3929, 2022.
[202] J. Welzel et al., "Optical coherence tomography of the human skin," *J. Amer. Acad. Dermatol.*, vol. 37, no. 6, pp. 958–963, 1997.
[203] X. Feng et al., "Functional imaging of human retina using integrated multispectral and laser speckle contrast imaging," *J. Biophotonics*, vol. 15, no. 2, 2022, Art. no. e202100285.
[204] L. Li et al., "Quantitative assessment of angiogenesis in skin wound healing by multi-optical imaging techniques," *Front. Phys.*, vol. 10, 2022, Art. no. 894901.
[205] V. Dremin et al., "Dynamic evaluation of blood flow microcirculation by combined use of the laser Doppler flowmetry and high-speed videocapillaroscopy methods," *J. Biophotonics*, vol. 12, no. 6, 2019, Art. no. e201800317.
[206] J. Chen et al., "Research progress on endoscopic multimodal optical imaging," *Opt. Laser Technol.*, vol. 191, 2025, Art. no. 113355.
[207] E. Pshenay-Severin et al., "Multimodal nonlinear endomicroscopic imaging probe using a double-core double-clad fiber and focus-combining micro-optical concept," *Light, Sci. Appl.*, vol. 10, no. 1, 2021, Art. no. 207.
[208] M. Hultman et al., "Real-time video-rate perfusion imaging using multi-exposure laser speckle contrast imaging and machine learning," *Proc. SPIE*, vol. 25, no. 11, 2020, Art. no. 116007.
[209] M. Hultman et al., "Speed-resolved perfusion imaging using multi-exposure laser speckle contrast imaging and machine learning," *Proc. SPIE*, vol. 28, no. 3, 2023, Art. no. 036007.
[210] K. Basak et al., "Learning of speckle statistics for in vivo and noninvasive characterization of cutaneous wound regions using laser speckle contrast imaging," *Microvascular Res.*, vol. 107, pp. 6–16, 2016.
[211] Y. Wang et al., "Unsupervised and quantitative intestinal ischemia detection using conditional adversarial network in multimodal optical imaging," *Proc. SPIE*, vol. 9, no. 6, 2022, Art. no. 064502.
[212] S. Zanelli et al., "Risk assessment of diabetic retinopathy with machine and deep learning models with PPG signals and PWV," in *Proc. 45th Annu. Int. Conf. IEEE Eng. Med. Biol. Soc.*, 2023, pp. 1–5.
[213] R. Divya et al., "Cardiovascular risk detection using Harris Hawks optimization with ensemble learning model on PPG signals," *Signal, Image Video Process.*, vol. 17, no. 8, pp. 4503–4512, 2023.
[214] J. Meng et al., "WSA-MP-net: Weak-signal-attention and multi-scale perception network for microvascular extraction in optical-resolution photoacoustic microcopy," *Photoacoustics*, vol. 37, 2024, Art. no. 100600.
[215] P. W. Sweeney et al., "Unsupervised segmentation of 3D microvascular photoacoustic images using deep generative learning," *Adv. Sci.*, vol. 11, 2024, Art. no. 2402195.
[216] Z. Wang et al., "Sparse coding-enabled low-fluence multi-parametric photoacoustic microscopy," *IEEE Trans. Med. Imag.*, vol. 41, no. 4, pp. 805–814, Apr. 2022.
[217] R. Owen et al., "A framework for responsible innovation," in *Responsible Innovation: Managing the Responsible Emergence of Science and Innovation in Society*, 1st ed., R. Owen, J. Bessant, and M. Heintz, Eds. Hoboken, NJ, USA: Wiley, 2013, pp. 27–50.